

Topologically-enhanced exciton transport

Joshua J. P. Thompson,¹ Wojciech J. Jankowski,² Robert-Jan Slager,² and Bartomeu Monserrat¹

¹*Department of Materials Science and Metallurgy, University of Cambridge, 27 Charles Babbage Road, Cambridge CB3 0FS, United Kingdom*

²*Theory of Condensed Matter Group, Cavendish Laboratory, University of Cambridge, J.J. Thomson Avenue, Cambridge CB3 0HE, United Kingdom*

(Dated: October 3, 2024)

Excitons dominate the optoelectronic response of many materials. Depending on the timescale and host material, excitons can exhibit free diffusion, phonon-limited diffusion, or polaronic diffusion, and exciton transport often limits the efficiency of optoelectronic devices such as solar cells or photodetectors. We demonstrate that topological excitons exhibit enhanced diffusion in all transport regimes. Appealing to notions of quantum geometry, we find that topological excitons are generically larger and more dispersive than their trivial counterparts, promoting their diffusion. We apply this general theory to a range of organic polyacene semiconductors, and show that exciton transport increases four-fold when topological excitons are present. We also propose that non-uniform electric fields can be used to directly probe the quantum metric of excitons, providing an experimental window into a basic geometric feature of quantum states. Our results provide a new avenue to enhance exciton transport and reveal that the mathematical ideas of topology and quantum geometry can be important ingredients in designing next-generation optoelectronic technologies.

I. INTRODUCTION

Excitons, Coulomb-bound electron-hole pairs, dominate the optoelectronic responses in a multitude of semiconductors [1–3]. Prominent examples include organic semiconductors [4, 5] and low-dimensional semiconductors [6–8], each a vast and versatile family of compounds which host excitons with large binding energies that can reach hundreds of milli-electronvolts [4, 9]. The formation, dynamics, lifetime, and transport of excitons dictate the efficiency of a host of technological applications, from solar cells [10, 11] and light-emitting diodes [12, 13], to biosensors [14, 15]. From a material perspective, the chemical and structural diversity available in the design of organic semiconductors and low-dimensional semiconductors allows fine-tuning of the electronic and excitonic properties for tailor-made device applications [16].

Despite their promising tunability, one of the key limitations of organic semiconductors is the low mobility of excitons [9, 17, 18]. For example, low exciton mobility has been shown to inhibit the efficiency of organic semiconductor based solar cells [19] since excitons decay before being extracted. As another example, in some organic systems the fission of optically active singlet excitons into pairs of optically inactive triplet excitons could help boost efficiency [11], but the diffusion of these triplets is even slower than that of singlets [18], and again exciton transport is a limiting factor. Other schemes, such as organic co-crystals [20, 21] and organic-inorganic interfaces [22, 23], again suffer from transport limitations.

A promising avenue for resolving such limitations is offered by topology. The topology of electrons is well-established [24–26], exhibiting remarkable transport properties. A natural question to ask is whether topological ideas can be extended to excitons, which are starting to be explored in two-dimensional van der Waals layered materials [27, 28], organic semiconductors [29], and models [30, 31]. In this context, particular attention has focused on topologically-induced non-trivial Riemannian geometry of exciton wavefunctions. It has been demonstrated that exciton quantum geometry,

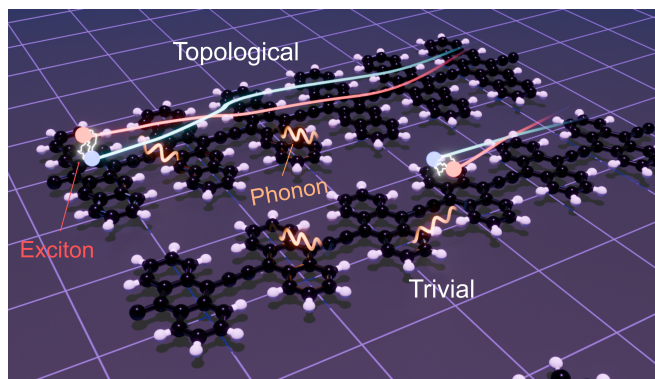


FIG. 1. Topologically-enhanced diffusive transport of topological excitons with inversion symmetry-protected topological \mathbb{Z}_2 -invariant P_{exc} in the presence of phonons (wiggly lines). Due to exciton-phonon interactions, the propagating excitons in topological excitonic band can be scattered, dephased, and the diffusive transport of the excitons can be further altered with non-uniform electric fields introducing a controllable forcing. We show that non-trivial excitonic quantum geometry can be manifested in all these transport features.

phrased in terms of the quantum metric [32], provides a lower bound on the centre-of-mass spread ξ of excitons [29]:

$$\xi^2 \geq \frac{a^2 P_{\text{exc}}^2}{4}, \quad (1)$$

where a is the lattice parameter of the crystal and P_{exc} is an excitonic topological invariant protected by crystalline inversion symmetry. We emphasise that these relations between topology, quantum geometry, and exciton properties are model independent and can be applied to different invariants in different dimensions and in different material platforms [33]. For example, in a one-dimensional setting, exemplified by organic polyacenes [29, 34, 35], the excitonic topology can be characterised through a topological invariant $P_{\text{exc}} \in \mathbb{Z}_2$, associated with the first Stiefel-Whitney characteristic class $w_1 \in \mathbb{Z}_2$ that reflects the unorientability of an excitonic band [29, 36, 37].

Qualitatively, the result in Eq. (1) implies that topological excitons are more delocalised, and can be *larger*, than their trivial counterparts. In this work, we exploit this key insight to demonstrate that topological excitons exhibit enhanced transport compared to their trivial counterparts. Similarly to the quantum geometric bound on exciton sizes, the topologically-enhanced transport properties are general. Nonetheless, we illustrate these results in a family of organic polyacene crystals, where topological excitons drive a four-fold increase in their transport. The applicability of these ideas to general material platforms provides a new avenue for improving optoelectronic technologies.

II. TOPOLOGICAL EXCITONS: MODEL AND MATERIALS

To explore the role of topology on exciton transport, we focus on a prototypical one-dimensional system which has been predicted to host topological excitons [29]. This setting is exemplified by polyacene chains characterised by n -ring acene molecules, where $n = 3, 5, 7$, linked by a carbon-carbon bond on the central carbon atoms. An illustrative example, polypentacene ($n = 5$), is shown in Fig. 1. The topology of the excitons in one-dimensional centrosymmetric semiconductors can be characterised with the exciton \mathbb{Z}_2 invariant P_{exc} , and they exhibit a topologically trivial exciton phase with $P_{\text{exc}} = 0$ for $n = 3$, and a topological phase with $P_{\text{exc}} = 1$ for $n = 5$ [29].

From a theoretical point of view, the electron properties of these polyacenes are accurately described through the Su-Schrieffer-Heeger (SSH) one-dimensional model [38, 39]:

$$H = -t_1 \sum_j c_{B,j}^\dagger c_{A,j} - t_2 \sum_j c_{B+1,j}^\dagger c_{A,j} + \text{h.c.}, \quad (2)$$

with $c_{B,j}^\dagger/c_{A,j}$ the creation/annihilation operators for the electrons at sublattices A, B , in unit cell j , and alternating hopping parameters t_1 and t_2 . In the polyacenes, the intracell t_1 coupling corresponds to hopping across the acene molecule and the intercell t_2 coupling to hoppings across the C-C double bond between molecules. In this language, the topological phase realising topological edge states, corresponds to $t_2 > t_1$, and the trivial phase corresponds to $t_2 < t_1$ [38, 39]. The exciton properties of these polyacenes can be described through the numerical solution of the Wannier equation [23, 29, 40], which directly incorporates the electron-hole Coulomb interaction. The topological invariant of excitons (P_{exc}) can be then directly obtained from the excitonic states [29].

We emphasise that the model and materials described above are only for illustrative purposes, and the key findings of this work are generally applicable to the transport of topological excitons in any material.

III. FREE EXCITON PROPAGATION

Following photoexcitation, excitons exhibit ultrafast ballistic-like transport at femtosecond timescales [41–43].

Microscopically, an exciton wavepacket initially forms around the photoexcitation spot. Subsequently, the wavepacket expands, which can be described by the hopping of exciton states between neighbouring lattice sites (see Methods). We calculate the hopping driven exciton transport for topological excitons ($t_2 > t_1$) and trivial excitons ($t_2 < t_1$), as shown in Fig. 2. The diffusion of topological excitons is significantly larger than that of their trivial counterparts, as characterised by their time-dependent spatial spread in Figs. 2(a) and 2(b). The values of t_1 and t_2 used in Fig. 2 correspond to the polypentacene $n = 5$ chain, which hosts topological excitons, and therefore our results demonstrate that exciton diffusion is enhanced in polypentacene driven by the underlying exciton topology.

To further quantify exciton transport, we use the exciton spread $\sigma_v^2(t) = \int dR R^2 |\psi_v^{\text{exc}}(R, t)|^2$, where v is an exciton band index and $\psi_v^{\text{exc}}(R, t) = \int dr \langle r, R | \psi_v^{\text{exc}}(t) \rangle$ is the exciton wave function in terms of the centre-of-mass coordinate R . $\psi_v^{\text{exc}}(R, t)$ accounts for all possible relative positions r of the electrons and holes. We define the exciton dispersion parameter α_v as:

$$\alpha_v = \partial_t \langle \delta x(t) \rangle_v \equiv \partial_t \left[\sqrt{\sigma_v^2(t) - \sigma_v^2(0)} \right], \quad (3)$$

which at its steady-state maximum value reflects the effective exciton mass $m_v^* \approx \hbar / \alpha_v \sigma_0$ associated with band v [44]. Here, $\langle \delta x(t) \rangle_v$ denotes a time-dependent effective displacement of the wavepacket wavefront. We depict the time evolution of α_v in Fig. 2(c) for the topological (solid line) and trivial (dashed line) excitons. Due to the frustration in the initial population, we see an initial acceleration of the exciton diffusion before saturating at a steady rate in both cases. Quantitatively, α_v is approximately three times larger in the topological case compared to the trivial case.

We attribute the enhanced transport exhibited by topological excitons to the lower bound on the exciton centre-of-mass spread, which makes topological excitons larger and therefore facilitates diffusion. Mathematically, quantum geometry reflects the Riemannian structure of the bundles of quantum states by inducing a quantum distance measure: $ds^2 \equiv g_{ij}^{\mu\nu}(Q) dQ^i dQ^j$ (see Methods). Physically, quantum geometry has been related to optics [33, 45] and spectral functions [33], which directly highlights its potential relevance to transport properties. In one spatial dimension, the quantum metric of excitons is defined in terms of interband matrix elements with band indices μ and ν as $g_{xx}^{\mu\nu}(Q) = \langle \partial_Q u_{\mu Q}^{\text{exc}} | u_{\nu Q}^{\text{exc}} \rangle \langle u_{\nu Q}^{\text{exc}} | \partial_Q u_{\mu Q}^{\text{exc}} \rangle$, where $|u_{\nu Q}^{\text{exc}}\rangle$ is the cell-periodic part of the exciton Bloch states. Tracing over the interband contributions, we can define the quantum metric associated with exciton band ν averaged over the Brillouin zone, namely $\langle g_{xx}^{\nu\nu}(Q) \rangle$. This quantity has been shown to satisfy a topological bound [29]:

$$\langle g_{xx}^{\nu\nu}(Q) \rangle \equiv \sum_{\mu \neq \nu} \langle g_{xx}^{\mu\nu}(Q) \rangle \geq \frac{a^2}{4} P_{\text{exc}}^2, \quad (4)$$

which drastically modifies the exciton transport, as we demonstrate here and in the following.

Figure 2 shows sub-picosecond transport, which showcases the difference in excitonic effective masses m_v^* of topological

and trivial excitons, as follows from the quantum geometric bound (see Methods). Exciton dynamics at longer timescales is dominated by phonon scattering (see below), but it is still interesting to explore the purely free exciton diffusion at these longer timescales [46]. For times $t > 1$ ps, we use Fokker-Planck dynamics induced by the Heisenberg equation of motion, as satisfied by the exciton density operators [see Supplemental Material (SM)], to describe free exciton diffusion according to:

$$\langle \delta x(t) \rangle_v = \sqrt{2D_v t} \geq \sqrt{\frac{2}{\hbar} \sum_{\mu \neq v} \langle \Delta_Q^{\mu v} g_{xx}^{\mu v}(Q) \rangle t}, \quad (5)$$

where $\Delta_Q^{\mu v}$ is the energy difference between exciton bands v and μ (see Methods). Connecting the diffusivity to the effective mass, $D_v = \hbar/2m_v^*$ (see Methods and SM [47, 48]), which is also related to the dispersion parameter α_v through m_v^* [44], this relation further reveals the importance of the geometric contribution to free exciton propagation.

We confirm this bound numerically by finding that the diffusivity of excitons in polyacenes is always above the topologically-bounded value of $D_v = 0.2$ cm²/s. We further confirm the validity of this bound by creating artificially flat bands for the polyacenes (see SM), and find that irrespective of the underlying electronic band dispersion, as long as the excitons are topological, the bound is obeyed.

IV. EXCITON TRANSPORT IN NON-UNIFORM ELECTRIC FIELDS

We next explore *driven* exciton transport under non-uniform electric fields, which we demonstrate can be used to directly probe the exciton quantum geometry. The exciton group velocity $\langle v_{vQ} \rangle$ associated with band v is given in one dimension (see Methods) by:

$$\langle v_{vQ} \rangle = \langle v_{vQ}^0 \rangle - \sum_{\mu \neq v} \frac{e^2}{\hbar^2} \partial_Q \left(\frac{g_{xx}^{\mu v}(Q)}{\Delta_Q^{\mu v}} \right) \left(\langle r \rangle \cdot \nabla_R \mathcal{E}(R) \right)^2, \quad (6)$$

where the electric field gradient $\nabla_R \mathcal{E}(R)$ couples to the electron-hole distance $\langle r \rangle$. According to Eq. (6), the total exciton group velocity has a contribution from the free exciton group velocity $\langle v_{vQ}^0 \rangle$, and a contribution from the quantum metric derivatives. In one dimension, the latter can be described by the Christoffel symbols $\Gamma_{xx}^{\mu v}(Q) = \frac{1}{2} \partial_Q g_{xx}^{\mu v}(Q)$. Overall, an exciton moving in a non-uniform electric field experiences a force, leading to either acceleration or deceleration of the exciton, and a modulation of the exciton group velocity.

The geometric contribution to the exciton group velocity in Eq. (6) depends on the energy difference $\Delta_Q^{\mu v}$ between bands μ and v . This dependence can be suppressed by increasing dielectric screening, for example through strongly polar substrates, such that $\Delta_Q^{\mu v} \approx \Delta$ can be made approximately uniform over the exciton Brillouin zone. In this regime, the non-linear exciton transport in non-uniform electric fields is directly given by the quantum geometric Christoffel symbols.

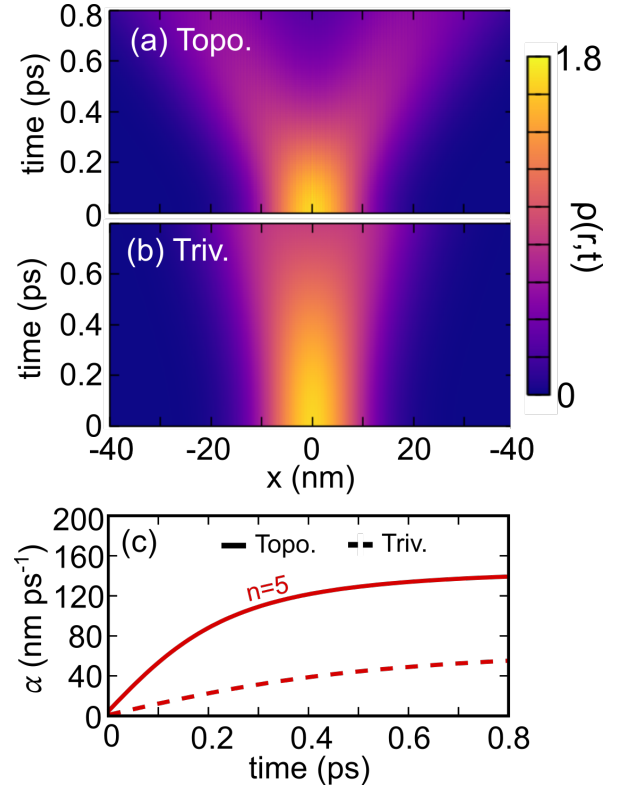


FIG. 2. Time-dependent transport of topologically non-trivial (a) and trivial (b) excitons. The diffusivity of topologically non-trivial excitons is bounded from below by the excitonic \mathbb{Z}_2 invariant. Parameters for $n = 5$ polyacene are used, with the DFT predicted combination of intracell (t_1) and intercell (t_2) hoppings employed in (a) while the order is flipped in (b), to truly ascertain the impact of topology. (c) Comparison of the excitons dispersion constant of the topological (solid) and trivial excitons (dashed) in polyacene ($n = 5$).

In Fig. 3(a), we schematically show the impact of an applied non-uniform electric field on exciton transport. For a more quantitative analysis, we perform a numerical simulation of the exciton group velocity for polyacene, where we also vary t_2 freely, and for simplicity we set the electric field gradient to be constant $\nabla_R \mathcal{E}(R) = 0.1$. Figure 3(b) shows the ratio between the group velocity \tilde{v}_Q modulated by a non-uniform electric field, and the group velocity v_Q in the absence of an external field. In the trivial regime, $\tilde{v}_Q/v_Q \approx 1$ due to the vanishing quantum metric $g_{xx}^{\mu v} \approx 0$ and vanishing variations thereof, $\Gamma_{xx}^{\mu v} \approx 0$. The topological regime ($t_2 > t_1$) shows a more complex behaviour. At small finite Q , the exciton diffusion is slowed down by the electric field with $\tilde{v}_Q/v_Q \approx 0$, as illustrated by the near white regions. At larger Q , the force induced by the non-uniform electric field on the topological excitons becomes even larger, leading to a *reversal* of the exciton velocity $\tilde{v}_Q/v_Q < 0$ until it exceeds the magnitude of the initial velocity in the opposite direction, $\tilde{v}_Q/v_Q < -1$. This effect is most significant for t_2 reasonably close to t_1 within the range $t_2 < 0.8$ eV. For larger t_2 , the exciton dispersion is flatter, leading to smaller excitons in real space.

Qualitatively, the distinct response of topological and triv-

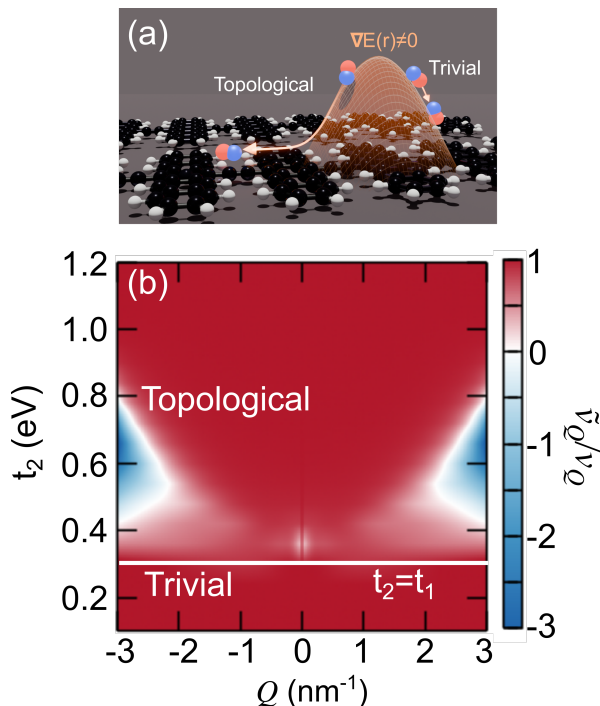


FIG. 3. (a) Schematic of non-uniform electric field on polypentacene crystal. The quantum metric of the topological exciton leads to a larger force due to the electric field compared to the trivial case. (b) Ratio of excitonic group velocity in the presence of and without a uniform electric field as a function of Q and t_2 . Here we set $\nabla_R \mathcal{E}(R) = \alpha = 0.1$ and $t_1 = 0.33$ eV, allowing us to define topological and trivial regimes, marked by the horizontal lines.

ial excitons under a non-uniform electric field can again be related to their different centre-of-mass localisations and relative sizes. Trivial excitons have a smaller size, and therefore they are less subject to electric field gradients. The quantum metric in the momenta conjugate to the relative electron-hole position r , and the centre-of-mass coordinates R , precisely reflect the corresponding spreads and localisations of excitons (see Methods).

V. PHONON-LIMITED EXCITON DIFFUSION

At picosecond timescales after photoexcitation, excitons no longer undergo free diffusion but instead experience phonon-limited diffusion, mediated by exciton-phonon interactions [49, 50].

Topological excitons can arise in two distinct scenarios in one-dimensional systems [29]. In the first, obstructed electrons and holes give rise to topological excitons; in the second, unobstructed electrons and holes can also give rise to topological excitons due to the electron-hole contribution [29, 30]. We find that in the first scenario, obstructed electrons and holes significantly enhance the exciton-phonon coupling of topological excitons. By contrast, topological excitons with unobstructed electrons and holes have a weak exciton-phonon coupling. Therefore, topological excitons arising from triv-

ial electrons and holes are the most mobile entities within all possible combinations of electron and exciton topologies.

To illustrate these results, Fig. 4(a-b) shows the exciton-phonon scattering matrix elements from an initial state Q to a final state Q' . We use dimensionless units, as we are interested in the impact of the overlap of exciton envelopes rather than the absolute values of electron-phonon coupling (see Methods). We observe different couplings for different momenta, depending on the topology associated with the Zak phases of the excitons, with the peak intensities being dictated by the quantum geometry of individual electrons and holes, as well as their momentum-dependent interaction. When $Q = Q'$, both topological and trivial cases give the ratios of the magnitudes of exciton-phonon coupling \mathcal{D} and electron-phonon coupling g matrix elements (see Methods) close to $|\mathcal{D}|^2/|g|^2 = 4$. When Q and Q' are both large and have the same sign, we find that the trivial case exhibits larger exciton-phonon coupling. However for Q and Q' with opposite signs, corresponding to a large momentum transfer, we see that the topological exciton-phonon scattering dominates.

One way to probe the impact of phonon scattering is via the exciton dephasing Γ_Q . When $Q = 0$, the dephasing corresponds to the non-radiative lifetime of the ground state. In Fig. 4(c), we present the exciton dephasing as a function of momentum for 50 K (orange) and 300 K (blue) for polypentacene. The solid and dashed lines show the trivial and topological regimes, respectively. The dephasing depends on the population of phonons, which increases as a function of temperature. As such the dephasing at 300 K is significantly larger than that at 50 K. Irrespective of temperature, the dephasing is lower in the topological case, which can be understood by the difference in the excitonic dispersion between the topological and trivial regimes, the latter being significantly shallower. This shallower excitonic band leads to a larger exciton density of states and to an increased number of available scattering channels. This competes with the enhanced exciton coupling that we expect in the topological phase, leading to an overall smaller dephasing. The bump at low Q occurs due to the temperature-activated onset of optical phonon scattering.

We calculate the phonon-limited exciton diffusion coefficients (see Methods) and report the results in Fig. 4(d). The reduced exciton-phonon dephasing and the higher exciton velocity associated with topological excitons lead to topological excitons diffusing about four times faster than trivial excitons at all temperatures. The temperature dependence is fairly typical [41, 49] and reflects the interplay between temperature increasing the population of fast excitons versus the enhanced exciton-phonon scattering at higher temperatures.

VI. POLARONIC EFFECTS

When the interaction between excitons and phonons becomes sufficiently large, excitons can become localised by the lattice [51, 52], becoming heavier and undergoing slower transport, as schematically illustrated in Fig. 5(a). These exciton-polarons have been studied extensively [53–55], and are particularly relevant in organic systems where their for-

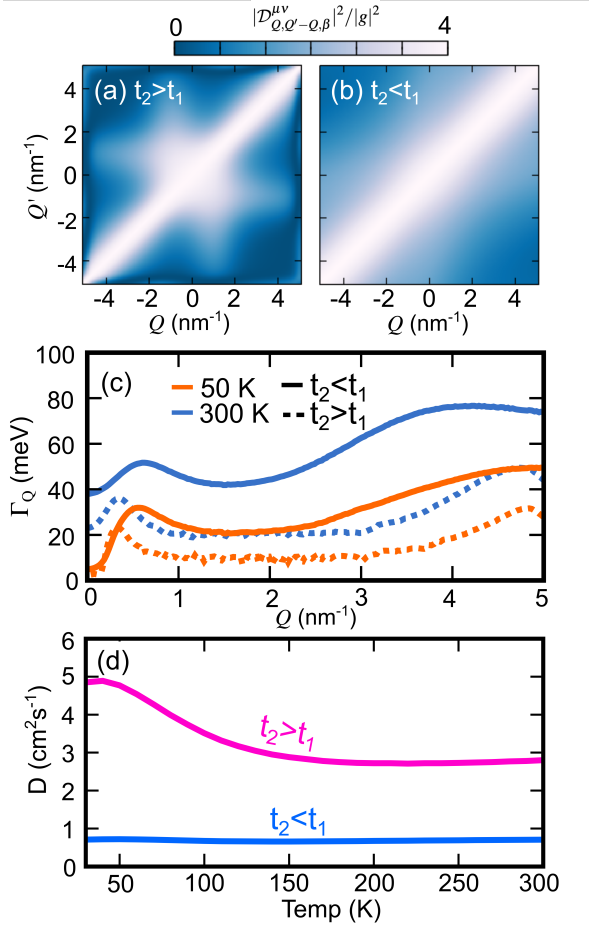


FIG. 4. Topology-dependent exciton-phonon coupling in polypentacene. **(a-b)** Exciton-phonon matrix elements resolved in initial Q and final Q' excitonic centre-of-mass momentum. **(c)** Phonon-induced exciton dephasing as function of initial momentum Q at 50 K (orange) and 300 K (blue). The trivial and topological exciton dephasings are shown by the solid and dashed lines respectively. **(d)** Phonon-stimulated exciton diffusion for trivial (blue) and topological (pink) excitons.

mation hinders the already limited energy transfer across organic optoelectronic devices [56]. Hence, understanding the transport of excitons in this regime is crucial.

We calculate the exciton band dispersion for polypentacene as renormalised by exciton-polarons at 300 K by treating the exciton-phonon interaction self-consistently (see Methods). The renormalised dispersion results in a decrease in the group velocity. In Fig. 5(b), we show the ratio of the free excitonic velocity to the polaronic group velocity. We find the usual low-momentum decrease of the exciton-polaron velocity ($v_{\text{Exc}}/v_{\text{Exc-Pol}} > 1$) in both the trivial (green) and topological (red) cases, corresponding to a polaron velocity around 70% of that of the free exciton. Notably, the topological exciton-polaron exhibits a decreased velocity, and a correspondingly increased mass, over a smaller momentum range, which we attribute to the reduced exciton density of states in the topological exciton dispersion. The corresponding band structures are shown in Figs. 5(c) and 5(d) for the trivial and

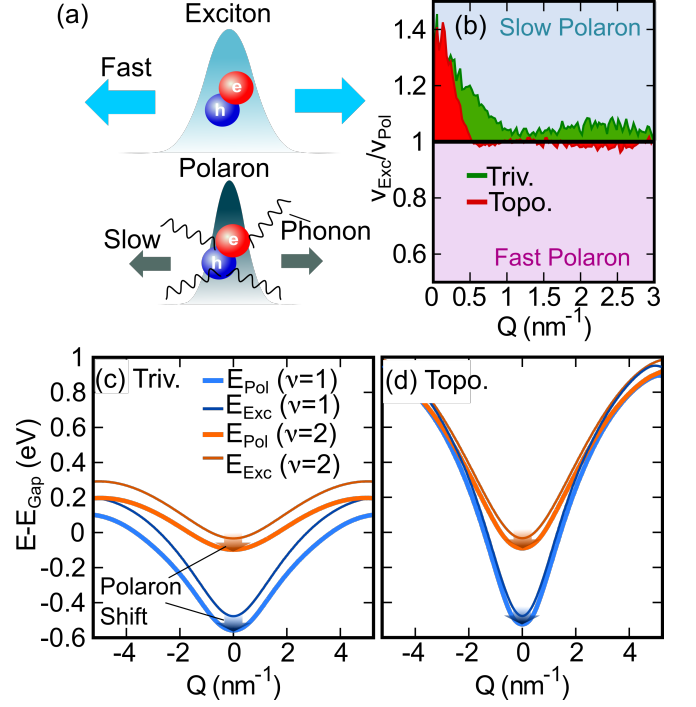


FIG. 5. Transport of topological exciton-polarons. **(a)** Schematic of reduced transport of exciton-polarons compared to bare excitons. **(b)** Ratio of free exciton to exciton-polaron group velocities in polypentacene at 300 K for trivial (green) and topological (red) regimes. The blue region indicates mass enhancement and slower exciton-polarons while the pink region indicates mass reduction and faster excitons. Corresponding exciton-polaron and exciton band dispersion is for **(c)** trivial and **(d)** topological excitons. A clear polaron shift is observed in both cases.

topological regimes, respectively. We observe the expected increase in the exciton effective mass and the corresponding reduction in the exciton group velocity, and we also see clear polaron energy shifts in both the topological and trivial cases. Experimentally, this will lead to a red-shift of the excitonic resonance energy [57] in the spectrum of absorbed/emitted light on a picosecond timescale. Importantly, the band topology of the exciton-polarons is the same as that of the bare excitons, and we note that at large Q the topological exciton-polaron bands are close in energy but do not cross, analogous to the bare exciton case. Our results show that, even in the polaronic regime, the transport of excitons is still significantly larger for topological excitons compared to their trivial counterparts.

VII. DISCUSSION

Overall, our results show that the topologically-bounded localisation properties of excitons dramatically affect their transport properties. Compared to their trivial counterparts, topological excitons sustain faster free transport, have lower effective masses, and their transport signatures are more robust to polaronic effects.

Topological excitons also have stronger electron-phonon coupling compared to their trivial counterparts. This observation respects the expected enhancement of electron-phonon coupling of the constituent electrons and holes that host non-trivial quantum geometry [58]. Nonetheless, we note that the non-trivial quantum geometry controlling the values of the electron-phonon coupling strength g is not a prerequisite for enhanced exciton-phonon coupling when the exciton topology arises from trivial electrons [29, 30]. This follows by noting that the exciton-phonon coupling strength includes the Q -dependent overlaps of the excitonic envelope functions $\psi_{vQ}(k)$, which can be solely responsible for the non-trivial excitonic geometry and topology [29]. As discussed earlier, while the stronger exciton-phonon coupling experienced by topological excitons results in higher dephasing rates, we find that these are not sufficient for the topological excitons to violate the original quantum geometric bounds of the free exciton propagation, as compared to the trivial excitons. Similarly, the computation of the polaronic effects shows that the modified transport of topological excitons is also robust against coupling to the lattice of organic crystals. These findings, accounting for the presence of physical effects present in all semiconducting materials, show that our diagnosis of quantum geometric manifestations on excitons should persist under the experimental conditions.

Finally, we stress that the exciton transport properties and the associated exciton quantum geometry and topology can be controlled using an appropriate dielectric environment [29], chemical modifications, and temperature, which modifies the population of the excitonic (and phonon) states. Therefore, our findings provide a more general quantum mechanical formalism and mathematical insights to theoretically understand the experimentally controllable geometric manifestations due to excitonic topologies, as reflected in the discussed excitonic transport in semiconductor materials.

VIII. CONCLUSIONS

We have demonstrated that the transport of topological excitons is significantly enhanced compared to that of trivial excitons. This discovery arises from the lower bound that the centre-of-mass excitonic quantum geometry sets on the exciton localisation, making topological excitons larger and therefore more mobile. We have shown that enhanced topological exciton transport holds in all regimes, including sub-picosecond free transport and longer timescales phonon-limited and polaronic transport. Additionally, we have illustrated these discoveries in a family of polyacene organic semiconductors. Our results are general, and we expect that exciton topology can be exploited to enhance the transport properties of a wide variety of semiconductors for applications in optoelectronic devices.

ACKNOWLEDGMENTS

The authors thank Richard Friend and Akshay Rao for helpful discussions. J.J.P.T. and B.M. acknowledge support from a EPSRC Programme Grant [EP/W017091/1]. W.J.J. acknowledges funding from the Rod Smallwood Studentship at Trinity College, Cambridge. R.-J.S. acknowledges funding from a New Investigator Award, EPSRC grant EP/W00187X/1, a EPSRC ERC underwrite grant EP/X025829/1, a Royal Society exchange grant IES/R1/221060, and Trinity College, Cambridge. B.M. also acknowledges support from a UKRI Future Leaders Fellowship [MR/V023926/1] and from the Gianna Angelopoulos Programme for Science, Technology, and Innovation.

IX. METHODS

A. Exciton quantum geometry

We consider an exciton wavefunction associated with exciton band ν and centre-of-mass momentum \mathbf{Q} :

$$|\psi_{\nu\mathbf{Q}}^{\text{exc}}\rangle = e^{i\mathbf{Q}\cdot\hat{\mathbf{R}}} |u_{\nu\mathbf{Q}}^{\text{exc}}\rangle, \quad (7)$$

where $\mathbf{R} = \frac{\mathbf{r}_e + \mathbf{r}_h}{2}$ is the center-of-mass coordinate, and \mathbf{r}_e and \mathbf{r}_h are the individual electron and hole coordinates. The exciton wavefunction satisfies Bloch's theorem under translational symmetry, and the cell-periodic part is given by:

$$|u_{\nu\mathbf{Q}}^{\text{exc}}\rangle = e^{-i\mathbf{Q}\cdot\hat{\mathbf{R}}} \sum_{\mathbf{k}} e^{i\mathbf{k}\cdot\hat{\mathbf{r}}} \psi_{\nu\mathbf{Q}}(\mathbf{k}) |u_{\mathbf{k}+\mathbf{Q}/2}^e\rangle |u_{-\mathbf{k}+\mathbf{Q}/2}^h\rangle \equiv e^{-i\mathbf{Q}\cdot\hat{\mathbf{R}}} \sum_{\mathbf{k}} e^{i\mathbf{k}\cdot\hat{\mathbf{r}}} |u_{\nu\mathbf{Q},\mathbf{k}}^{\text{exc}}\rangle. \quad (8)$$

In this expression, $\mathbf{r} = \mathbf{r}_e - \mathbf{r}_h$ is the relative electron-hole coordinate, $|u_{\mathbf{k}+\mathbf{Q}/2}^e\rangle$ and $|u_{-\mathbf{k}+\mathbf{Q}/2}^h\rangle$ are the single-particle electron and hole states, and $\psi_{\nu\mathbf{Q}}(\mathbf{k})$ is the envelope function capturing the electron-hole interactions.

The quantum geometry associated with exciton states was originally introduced in Ref. [29]. The quantum geometric tensor in the centre-of-mass coordinates $(\mathbf{R})_i \sim i\partial_{Q_i}$ is given by:

$$\mathcal{Q}_{ij}^{\text{exc},\nu}(\mathbf{Q}) = \langle \partial_{Q_i} u_{\nu\mathbf{Q}}^{\text{exc}} | (1 - \hat{P}_{\nu\mathbf{Q}}) | \partial_{Q_j} u_{\nu\mathbf{Q}}^{\text{exc}} \rangle, \quad (9)$$

where $\hat{P}_{\nu\mathbf{Q}} = |u_{\nu\mathbf{Q}}^{\text{exc}}\rangle \langle u_{\nu\mathbf{Q}}^{\text{exc}}|$ is a projector onto the exciton band of interest. Its real part, the quantum metric, is given by:

$$g_{ij}^{\text{exc},\nu}(\mathbf{Q}) = \frac{\langle \partial_{Q_i} u_{\nu\mathbf{Q}}^{\text{exc}} | (1 - \hat{P}_{\nu\mathbf{Q}}) | \partial_{Q_j} u_{\nu\mathbf{Q}}^{\text{exc}} \rangle + \langle \partial_{Q_j} u_{\nu\mathbf{Q}}^{\text{exc}} | (1 - \hat{P}_{\nu\mathbf{Q}}) | \partial_{Q_i} u_{\nu\mathbf{Q}}^{\text{exc}} \rangle}{2}, \quad (10)$$

and it relates to the centre-of-mass spread of excitons $\langle (\mathbf{R} - \langle \mathbf{R} \rangle)^2 \rangle$. Importantly, the relation between the exciton spread and the quantum metric can be exploited to reconstruct the exciton quantum metric in time-dependent transport experiments that involve freely propagating and driven excitons, as we show in the main text.

Moreover, using the exciton wavefunction, a quantum geometric tensor in the relative coordinate $(\mathbf{r})_i \sim i\partial_{k_i}$ can be defined as:

$$\mathcal{Q}_{ij,\mathbf{Q}}^{\text{exc},\nu}(\mathbf{k}) = \langle \partial_{k_i} u_{\nu\mathbf{Q},\mathbf{k}}^{\text{exc}} | (1 - \hat{P}_{\nu\mathbf{Q},\mathbf{k}}) | \partial_{k_j} u_{\nu\mathbf{Q},\mathbf{k}}^{\text{exc}} \rangle, \quad (11)$$

where $\hat{P}_{\nu\mathbf{Q},\mathbf{k}} = |u_{\nu\mathbf{Q},\mathbf{k}}^{\text{exc}}\rangle \langle u_{\nu\mathbf{Q},\mathbf{k}}^{\text{exc}}|$ is the projector onto the considered excitonic states. Its real part, the quantum metric, reads:

$$g_{ij,\mathbf{Q}}^{\text{exc},\nu}(\mathbf{k}) = \text{Re } \mathcal{Q}_{ij,\mathbf{Q}}^{\text{exc}}(\mathbf{k}) = g_{ij,\mathbf{Q}}^{\text{exc,en},\nu}(\mathbf{k}) + g_{ij,\mathbf{Q}}^{\text{exc,sp},\nu}(\mathbf{k}) + g_{ij,\mathbf{Q}}^{\text{exc,en-sp},\nu}(\mathbf{k}), \quad (12)$$

where the individual contributions arise from the envelope function:

$$g_{ij,\mathbf{Q}}^{\text{exc,en},\nu}(\mathbf{k}) = \text{Re } \sum_{\mathbf{k}} \partial_{k_i} \psi_{\nu\mathbf{Q}}^*(\mathbf{k}) \partial_{k_j} \psi_{\nu\mathbf{Q}}(\mathbf{k}) - \text{Re } \sum_{\mathbf{k},\mathbf{k}'} [\psi_{\nu\mathbf{Q}}(\mathbf{k}) \partial_{k_i} \psi_{\nu\mathbf{Q}}^*(\mathbf{k})] [\psi_{\nu\mathbf{Q}}^*(\mathbf{k}') \partial_{k_j} \psi_{\nu\mathbf{Q}}(\mathbf{k}')], \quad (13)$$

from the single-particle terms:

$$g_{ij,\mathbf{Q}}^{\text{exc,sp},\nu}(\mathbf{k}) = \frac{1}{4} \sum_{\mathbf{k}} |\psi_{\nu\mathbf{Q}}(\mathbf{k})|^2 \left[g_{ij}^e(\mathbf{k} + \mathbf{Q}/2) + g_{ij}^h(\mathbf{k} - \mathbf{Q}/2) \right] - A_{\nu\mathbf{Q}}^{\text{exc,sp},i} A_{\nu\mathbf{Q}}^{\text{exc,sp},j}, \quad (14)$$

and from a mixed envelope-single-particle contribution:

$$g_{ij,\mathbf{Q}}^{\text{exc,en-sp},\nu}(\mathbf{k}) = \frac{1}{2} \sum_{\mathbf{k}} \left[\partial_{k_i} |\psi_{\nu\mathbf{Q}}(\mathbf{k})|^2 \partial_{k_j} A_{\text{exc}}^{\text{sp},i} + \partial_{k_j} |\psi_{\nu\mathbf{Q}}(\mathbf{k})|^2 \partial_{k_i} A_{\nu\mathbf{Q}}^{\text{exc,sp},j} \right] - \left[A_{\nu\mathbf{Q}}^{\text{exc,sp},i} A_{\nu\mathbf{Q}}^{\text{exc},j} + A_{\nu\mathbf{Q}}^{\text{exc},i} A_{\nu\mathbf{Q}}^{\text{exc,sp},j} \right]. \quad (15)$$

In these expressions, the exciton Berry connection in the *relative* coordinate is given by $A_{\nu\mathbf{Q}}^{\text{exc}}(\mathbf{k}) = i \langle u_{\nu\mathbf{Q},\mathbf{k}}^{\text{exc}} | \nabla_{\mathbf{k}} u_{\nu\mathbf{Q},\mathbf{k}}^{\text{exc}} \rangle = A_{\nu\mathbf{Q}}^{\text{exc,sp}}(\mathbf{k}) + A_{\nu\mathbf{Q}}^{\text{exc,en}}(\mathbf{k})$, with the single-particle part $A_{\nu\mathbf{Q}}^{\text{exc,sp}}(\mathbf{k}) = A_{\nu}^e(\mathbf{k} + \mathbf{Q}/2) + A_{\nu}^h(\mathbf{k} - \mathbf{Q}/2)$, and the envelope part $A_{\nu\mathbf{Q}}^{\text{exc,en}}(\mathbf{k}) = i \psi_{\nu\mathbf{Q}}^*(\mathbf{k}) \nabla_{\mathbf{k}} \psi_{\nu\mathbf{Q}}(\mathbf{k})$. Additionally, $g_{ij}^{e/h}(\mathbf{k})$ are the individual single-particle quantum metrics of the electrons and holes constituting the excitonic states.

The excitonic quantum metric associated with the relative coordinate relates to the standard deviation of the electron-hole separation $\langle (\mathbf{r} - \langle \mathbf{r} \rangle)^2 \rangle$ in the exciton state [59].

B. Time-dependent free exciton propagation

In this section we derive the spatiotemporal dynamics of excitons in a one-dimensional Su–Schrieffer–Heeger (SSH) chain, following the approach of Ref. [44].

The exciton Wannier function $|w_{R_m}^\mu\rangle$ associated with the centre-of-mass position $\langle X \rangle$ of an exciton in unit cell m is given by:

$$|w_{R_m}^\mu\rangle = \frac{1}{\sqrt{N}} \int_{\text{BZ}} dQ \exp\left(i(X + ma)Q\right) |u_{Q\mu}^{\text{exc}}\rangle \quad (16)$$

where a is the lattice constant of the SSH chain and $|u_{Q\mu}^{\text{exc}}\rangle$ is the excitonic wavefunction defined over centre of mass momenta Q .

The overlap of neighbouring Wannier functions gives a measure of the coupling, and hence ‘‘hopping’’ rate, between neighbouring sites. We define a hopping Hamiltonian between excitons with distinct centre-of-mass position:

$$\hat{H}_{\text{free}} = \sum_{m,n} t_{nm}^v \hat{X}_{nv}^\dagger \hat{X}_{mv}, \quad (17)$$

where the hopping parameter is given by:

$$t_{nm}^v = \int dx \langle w_{R_n}^v | H | w_{R_m}^v \rangle = \frac{1}{N} \sum_Q E_{vQ} e^{iQ(R_m - R_n)}. \quad (18)$$

We note that $\varepsilon_v = t_{nn}^v$ is the onsite energy of the exciton at lattice site n .

The spatial profile of the exciton distribution is given by:

$$\rho^v(x, t) = \sum_{n,m} \rho_{nm}^v \langle w_{R_m}^v | w_{R_n}^v \rangle, \quad (19)$$

where $\rho_{nm}^v = \langle \hat{X}_{nv}^\dagger \hat{X}_{mv} \rangle$ is the density matrix. The time evolution of the density matrix is described by the Heisenberg equation of motion [44]:

$$\partial_t \rho_{nm}^v = -\frac{i}{\hbar} \sum_j (t_{mj}^v \rho_{nj} - t_{jn}^v \rho_{jm}). \quad (20)$$

Solving this set of differential equations and substituting into Eq. (19), we obtain the spatial evolution of the exciton distribution.

To further address the free exciton diffusion beyond the sub-ps timescales, as presented in Fig. 2, we assume a Gaussian-like excitation spot which gives an initial Gaussian distribution following optical excitation. In this setting, the off-diagonal terms vanish, $\rho_{nm \neq n}^v(t=0) = 0$, and the diagonal terms read [44]:

$$\rho_{nn}^v(t=0) = \frac{1}{\sqrt{2\pi\sigma_{\text{Ini}}^2}} \exp\left(\frac{-(na - x_{\text{Ini}})^2}{2\sigma_{\text{Ini}}^2}\right), \quad (21)$$

where x_{Ini} and σ_{Ini} are the initial excitation centre and broadening, respectively. Following Fick’s second law, the temporal and spatial evolution of the exciton density can be expressed as:

$$\rho^v(x, t) = \frac{N_0}{\sqrt{2\pi(2D_v t + w_0^2)}} \exp\left[\frac{-(x - x_{\text{Ini}})^2}{2(2D_v t + w_0^2)}\right], \quad (22)$$

where N_0 is the initial number of generated excitons in excitonic band v , and for well-localised excitons we have $w_0^2 \approx \sigma_{\text{Ini}}^2$.

In the following, we show that the exciton diffusivity D_v in band v is fully captured by the centre-of-mass quantum metric of the excitons $g_{xx}(Q)$. By fitting Fokker-Planck Gaussian propagation in one spatial dimension, we obtain that $\sigma^2(t) = \sigma_{\text{Ini}}^2 + 2D_v t$, with $D_v = \frac{\hbar}{2m_v^*} \rightarrow \langle g_{xx}^v(Q) \rangle$. The full derivation is detailed in the Supplemental Material (SM), but briefly, we map the density time-evolution equation to the Fokker-Planck equation, in order to connect the diffusivity to the effective excitonic mass m_v^* . Furthermore, we utilise the Hellmann-Feynman theorem to derive the relation between the effective excitonic mass (m_v^*) and the quantum-geometry in the centre-of-mass momentum space. As a result, we find that the diffusivity of excitons in band v is given by:

$$D_v = \frac{1}{2\hbar} \left\langle \frac{\partial^2 E_{vQ}}{\partial Q^2} \right\rangle + \frac{1}{\hbar} \sum_{\mu \neq v} \langle \Delta_Q^{\mu v} g_{xx}^{\mu v}(Q) \rangle, \quad (23)$$

where E_{vQ} is a dispersion of band v , and the averages are taken with respect to the Brillouin zone spanned in the Q momentum space parameter. For topological excitons, we further employ the quantum geometric bound [29]:

$$\langle g_{xx}^v(Q) \rangle \geq \frac{a^2}{4} P_{\text{exc}}, \quad (24)$$

with the \mathbb{Z}_2 excitonic invariant $P_{\text{exc}} = 0, 1$. Assuming that the exciton band dispersion exhibits non-negative average curvature, as is the case for example in the studied polyacenes under arbitrary dielectric environment, we obtain:

$$\langle \delta x(t) \rangle_v = \sqrt{2D_v t} \geq \sqrt{\frac{2t}{\hbar} \sum_{\mu \neq v} \langle \Delta_Q^{\mu v} g_{xx}^{\mu v}(Q) \rangle} \geq \sqrt{\frac{2t}{\hbar} \min_{\mu \neq v} \Delta_Q^{\mu v} \langle g_{xx}^v(Q) \rangle} \geq \frac{a}{2} \sqrt{\frac{2t}{\hbar} \min_{\mu \neq v} \Delta_Q^{\mu v}}. \quad (25)$$

We note that the first inequality saturates in the flat excitonic band limit. We numerically observe that for arbitrary t_1 and t_2 , the bound is satisfied across time t , saturating to the value dependent only on the size of the band gaps $\Delta_Q^{\mu v}$ and the lattice constant a (see also SM).

C. Driven exciton transport under non-uniform electric fields

We consider exciton transport driven by an external non-uniform electric field gradient, complementary to the field gradients realisable internally within the system [60]. Semiclassically, interacting electrons and holes satisfy the equation of motion [61]:

$$\dot{\mathbf{k}}_{e/h} = -\nabla_{\mathbf{r}_{e/h}} U(\mathbf{r}_e - \mathbf{r}_h) \mp e\mathcal{E}(\mathbf{r}_{e/h}), \quad (26)$$

where $U(\mathbf{r}_e - \mathbf{r}_h)$ is the electron-hole interaction potential. This implies that the centre-of-mass exciton momentum $\mathbf{Q} = \mathbf{k}_e + \mathbf{k}_h$ satisfies an equation of motion with a position-dependent external force $\mathbf{F}(\mathbf{R})$:

$$\dot{\mathbf{Q}} = e[\mathcal{E}(\mathbf{r}_h) - \mathcal{E}(\mathbf{r}_e)] = e[\mathcal{E}(\mathbf{R} + \mathbf{r}/2) - \mathcal{E}(\mathbf{R} - \mathbf{r}/2)] = e\langle \mathbf{r} \rangle \cdot \nabla_{\mathbf{R}} \mathcal{E}(\mathbf{R}) = \mathbf{F}(\mathbf{R}). \quad (27)$$

In this expression, we use $\mathbf{R} = (\mathbf{r}_e + \mathbf{r}_h)/2$, $\mathbf{r} = \mathbf{r}_e - \mathbf{r}_h$ and that to first order, $\mathcal{E}(\mathbf{R} \pm \mathbf{r}/2) = \mathcal{E}(\mathbf{R}) \pm \mathbf{r}/2 \cdot \nabla_{\mathbf{R}} \mathcal{E}(\mathbf{R}) + O(r^2)$.

Physically, the quantum geometric coupling to $\dot{\mathbf{Q}}$ can be related to the renormalised exciton energies. Consider a perturbation coupling to the centre of mass of the exciton $\Delta H = -\mathbf{R} \cdot \mathbf{F}(\mathbf{R})$, where \mathbf{R} is a position operator projected onto an excitonic band. For the off-diagonal elements, we have $\langle \psi_{\mu\mathbf{Q}}^{\text{exc}} | \mathbf{R} | \psi_{\nu\mathbf{Q}}^{\text{exc}} \rangle = i \langle u_{\mu\mathbf{Q}}^{\text{exc}} | \nabla_{\mathbf{Q}} u_{\nu\mathbf{Q}}^{\text{exc}} \rangle$, whereas the diagonal elements vanish by parity. At second order in perturbation theory, and assuming that the exciton bands are non-degenerate, we obtain the following energy corrections:

$$\tilde{E}_{\nu\mathbf{Q}} = E_{\nu\mathbf{Q}} - \sum_{\mu \neq \nu} \frac{|\langle \psi_{\nu\mathbf{Q}}^{\text{exc}} | \Delta H | \psi_{\mu\mathbf{Q}}^{\text{exc}} \rangle|^2}{E_{\mu\mathbf{Q}} - E_{\nu\mathbf{Q}}} = E_{\nu\mathbf{Q}} - \sum_{\mu \neq \nu} \frac{\mathbf{F}^T(\mathbf{R}) \cdot \langle \psi_{\nu\mathbf{Q}}^{\text{exc}} | \mathbf{R} | \psi_{\mu\mathbf{Q}}^{\text{exc}} \rangle \langle \psi_{\mu\mathbf{Q}}^{\text{exc}} | \mathbf{R} | \psi_{\nu\mathbf{Q}}^{\text{exc}} \rangle \cdot \mathbf{F}(\mathbf{R})}{E_{\mu\mathbf{Q}} - E_{\nu\mathbf{Q}}}, \quad (28)$$

which in terms of the excitonic quantum metric, we can rewrite as

$$\tilde{E}_{\nu\mathbf{Q}} = E_{\nu\mathbf{Q}} - \sum_{\mu \neq \nu} \frac{g_{xx}^{\mu\nu}(Q)}{E_{\mu\mathbf{Q}} - E_{\nu\mathbf{Q}}} F(\mathbf{R}) F(\mathbf{R}), \quad (29)$$

for a one-dimensional system. Here, $\tilde{E}_{\nu\mathbf{Q}}$ is the excitonic energy renormalised by the coupling to external force fields. Denoting $\Delta_Q^{\mu\nu} = E_{\mu\mathbf{Q}} - E_{\nu\mathbf{Q}}$, and substituting $F(\mathbf{R}) = \hbar \dot{\mathbf{Q}} = e\langle \mathbf{r} \rangle \cdot \nabla_{\mathbf{R}} \mathcal{E}(\mathbf{R})$, we arrive at:

$$\langle v_{\nu\mathbf{Q}} \rangle = \frac{1}{\hbar} \partial_Q \tilde{E}_{\nu\mathbf{Q}} = \langle v_{\nu\mathbf{Q}}^0 \rangle - \sum_{\mu \neq \nu} \frac{e^2}{\hbar^2} \partial_Q \left(\frac{g_{xx}^{\mu\nu}(Q)}{\Delta_Q^{\mu\nu}} \right) \left(\langle \mathbf{r} \rangle \cdot \nabla_{\mathbf{R}} \mathcal{E}(\mathbf{R}) \right)^2 \quad (30)$$

where $\langle v_{\nu\mathbf{Q}}^0 \rangle = \frac{1}{\hbar} \partial_Q E_{\nu\mathbf{Q}}$ is the free exciton velocity.

The above result implies that varying the electric field gradient in transport experiments allows the reconstruction of the derivatives of the exciton quantum metric. As mentioned in the main text, in the flat-band limit $\Delta_Q^{\mu\nu} \approx \Delta$, the Christoffel symbols $\Gamma_{xxx}^{\mu\nu} = \frac{1}{2} \partial_Q g_{xx}^{\mu\nu}(Q)$ can be directly accessed with this strategy. It should be noted that the size of the exciton, given by the average of the relative electron-hole coordinate $\langle r \rangle$, must be known to assess the magnitude of the force $F(\mathbf{R})$ due to the electric field gradient $\nabla_{\mathbf{R}} \mathcal{E}(\mathbf{R})$. Correspondingly, we compute the average size of the exciton that is relevant for the semiclassical equation of motion directly from the envelope function: $\langle r \rangle = \int_0^\infty dr r \times |\psi_{\nu\mathbf{Q}}(r)|^2$, where $\psi_{\nu\mathbf{Q}}(r)$ is a Fourier transform of $\psi_{\nu\mathbf{Q}}(k)$ [29].

From the perspective of quantum geometry, we note that the derivatives of the quantum metric defining the Christoffel symbols can be in principle arbitrarily high due to the envelope contributions to the excitonic quantum metric, resulting in a nearly step-like character for $g_{xx}^{\text{exc}}(Q)$ in the presence of a singular non-Abelian Berry connection. Such singular behaviours of non-Abelian excitonic Berry connection are only to be expected in topological excitonic phases, as in the trivial phases with vanishing topological invariants the Berry connection can be chosen to be globally smooth.

D. Exciton-phonon coupling

We consider the connection between exciton-phonon coupling (ExPC) matrix elements [62] and quantum geometry. The electron-phonon coupling can be written as

$$H_{\text{el-ph}} = \sum_{k,\lambda,K,\beta} g_{kK\beta\lambda} \hat{a}_{\lambda,k+K}^\dagger \hat{a}_{\lambda k} \left(\hat{b}_{\beta,K} + \hat{b}_{\beta,-K}^\dagger \right), \quad (31)$$

where $\hat{a}_{\lambda k}^{(\dagger)}$ is the annihilation (creation) operator for an electron in band λ and momentum k . Similarly, $\hat{b}_{\beta q}^{(\dagger)}$ is the annihilation (creation) operator for a phonon with mode β and momentum K . The coupling between electrons and phonons is quantified by the matrix elements $g_{kK\beta\lambda}$. To make our discussion concrete, we will consider a two-band model with $\lambda = c$ and $\lambda = v$ denoting the conduction and valence bands, respectively. This regime is applicable to the polyacene chains discussed in the main text.

We define a pair operator basis as:

$$\hat{a}_{ck+K}^\dagger \hat{a}_{ck} = \sum_l \hat{P}_{k+K,l}^\dagger \hat{P}_{l,k}, \quad \hat{a}_{vk+K}^\dagger \hat{a}_{vk} = \sum_l \hat{P}_{l,k+K} \hat{P}_{k,l}^\dagger, \quad (32)$$

and we rewrite the electron-phonon coupling in this basis as:

$$H_{\text{el-ph}} = \sum_{k,l,K,\beta} \left(g_{kK\beta c} \hat{P}_{k+K,l}^\dagger \hat{P}_{l,k} + g_{kK\beta v} \hat{P}_{l,k+K} \hat{P}_{k,l}^\dagger \right) \left(\hat{b}_{\beta,K} + \hat{b}_{\beta,-K}^\dagger \right). \quad (33)$$

We can then re-write the Hamiltonian in the exciton basis:

$$H_{\text{ex-ph}} = \sum_{Q,K,\beta} \mathcal{D}_{QK\beta}^{\mu\nu} \hat{X}_{Q+K}^{\mu\dagger} \hat{X}_Q^\nu \left(\hat{b}_{\beta,K} + \hat{b}_{\beta,-K}^\dagger \right), \quad (34)$$

$$\mathcal{D}_{QK\beta}^{\mu\nu} = \sum_k \left(g_{kK\beta c} \psi_{Q+K\mu} \left(k - \frac{1}{2}Q + \frac{1}{2}K \right) \psi_{Q\nu}^* \left(k - \frac{1}{2}Q \right) - g_{kK\beta v} \psi_{Q+K\mu} \left(k + \frac{1}{2}Q - \frac{1}{2}K \right) \psi_{Q\nu}^* \left(k + \frac{1}{2}Q \right) \right), \quad (35)$$

where the electron-phonon coupling (EPC) matrix elements $g_{kK\beta v}$ reflect the quantum geometry of the underlying electrons and holes [58]. Contributions to ExPC explicitly originate from the free-particle EPC matrix elements ($g_{kK\beta v}$) and from the overlaps of excitonic envelope functions $\psi_Q(k)$ governed by the excitonic quantum geometry that was defined in the previous section, as we showcase in the following. For small phonon momentum K , we can expand in the exciton envelope function in the centre-of-mass momentum Q to first order:

$$\psi_{Q+K\mu} \left(k \pm \frac{1}{2}Q + \frac{1}{2}K \right) \approx \psi_{Q\mu} \left(k \pm \frac{1}{2}Q + \frac{1}{2}K \right) + K \cdot \partial_Q \psi_{Q\mu} \left(k \pm \frac{1}{2}Q + \frac{1}{2}K \right). \quad (36)$$

We also expand in the exciton relative momentum k associated with the relative coordinate r :

$$\begin{aligned} \psi_{Q+K\mu} \left(k - \frac{1}{2}Q + \frac{1}{2}K \right) \approx & \psi_{Q\mu} \left(k \pm \frac{1}{2}Q \right) + \frac{1}{2}K \cdot \nabla_k \psi_{Q\mu} \left(k \pm \frac{1}{2}Q \right) + K \cdot \partial_Q \psi_{Q\mu} \left(k \pm \frac{1}{2}Q \right) \\ & + (K \cdot \partial_Q) \left(\frac{1}{2}K \cdot \nabla_k \right) \psi_{Q\mu} \left(k \pm \frac{1}{2}Q \right). \end{aligned} \quad (37)$$

Neglecting the last term, which is second order in the phonon momentum, we can use the Berry connections in the centre-of-mass and relative coordinates: $A_{\nu\mathbf{k}}^{\text{exc, en}}(\mathbf{Q}) \equiv i\psi_{\nu\mathbf{Q}}^*(\mathbf{k})\nabla_{\mathbf{Q}}\psi_{\nu\mathbf{Q}}(\mathbf{k})$, $A_{\nu\mathbf{Q}}^{\text{exc, en}}(\mathbf{k}) \equiv i\psi_{\nu\mathbf{Q}}^*(\mathbf{k})\nabla_{\mathbf{k}}\psi_{\nu\mathbf{Q}}(\mathbf{k})$, to write:

$$\begin{aligned} \mathcal{D}_{QK\beta}^{\mu\nu} = & \sum_k \left(g_{kK\beta c} \left[\left| \psi_{Q\mu} \left(k - \frac{1}{2}Q \right) \right|^2 + K \cdot A_{\nu k - \frac{1}{2}Q}^{\text{exc, en}}(\mathbf{Q}) + \frac{1}{2}K \cdot A_{\nu\mathbf{Q}}^{\text{exc, en}} \left(k - \frac{1}{2}Q \right) \right] \right. \\ & \left. - g_{kK\beta v} \left[\left| \psi_{Q\mu} \left(k + \frac{1}{2}Q \right) \right|^2 + K \cdot A_{\nu k + \frac{1}{2}Q}^{\text{exc, en}}(\mathbf{Q}) + \frac{1}{2}K \cdot A_{\nu\mathbf{Q}}^{\text{exc, en}} \left(k + \frac{1}{2}Q \right) \right] \right), \end{aligned} \quad (38)$$

which explicitly shows that the exciton-phonon coupling depends on both the geometry in the centre-of-mass (R) and relative (r) exciton coordinate spaces. These are contributions beyond the inherited dependence from the individual electrons and holes arising from the electron-phonon coupling constants $g_{kK\beta\lambda}$ that reflect the quantum geometry of independent electrons and holes [58]. We note that away from the limit of small phonon momentum K , further geometric derivative terms in the expansion become important, as we numerically retrieve in the main text. In particular, we find that further geometric corrections become prominent in the $K \approx Q$ regime.

E. Dephasing driven by exciton-phonon coupling

In the presence of phonons, the exciton propagator becomes renormalised due to exciton-phonon coupling, and we can define an exciton self-energy as [63]:

$$\Sigma_{\mu Q} = - \lim_{\delta_0 \rightarrow 0} \sum_{K, \nu, \beta} |\mathcal{D}_{QK\beta}^{\mu\nu}|^2 \left(\frac{n_K^\beta + 1}{E_{\nu Q+K} - E_{\mu Q} + \hbar\Omega_{K\beta} + i\delta_0} + \frac{n_K^\beta}{E_{\nu Q+K} - E_{\mu Q} - \hbar\Omega_{K\beta} + i\delta_0} \right). \quad (39)$$

where $\Omega_{K\beta}$ is a frequency of a phonon with momentum K in band β , n_K^β is the occupation number capturing the population of the corresponding phonon mode, and δ_0 is an infinitesimal number introduced to shift the complex poles. The exciton dephasing rates due to phonons are given by the imaginary part of the self-energy, $\Gamma_{\mu Q} = \text{Im} \Sigma_{\mu Q}$, and we obtain the following expression:

$$\Gamma_{\mu Q} = \sum_{K, \nu, \beta} |\mathcal{D}_{QK\beta}^{\mu\nu}|^2 \left[(n_K^\beta + 1) \delta(E_{\nu Q+K} - E_{\mu Q} + \hbar\Omega_{K\beta}) + n_K^\beta \delta(E_{\nu Q+K} - E_{\mu Q} - \hbar\Omega_{K\beta}) \right]. \quad (40)$$

The dephasing at $Q = 0$ is the non-radiative contribution to the exciton linewidth due to phonons. Numerically, we solve the dephasing equation self-consistently [64], where the delta functions are treated as Lorentzians with width $\Gamma_{\mu Q} + \Gamma_{\nu Q+K}$. Physically, this takes into account the next highest-order scattering processes [64]. Dephasing for non-zero Q encodes the scattering rate of excitons by phonons, and enters the semi-classical exciton diffusion model in the presence of phonon scattering:

$$D_\mu^{\text{ph}} = \frac{1}{\mathcal{Z}} \sum_Q \frac{\langle v_{\mu Q} \rangle^2}{\Gamma_{\mu Q}} \exp\left(-\frac{E_{\mu Q}}{k_B T}\right), \quad (41)$$

where $\mathcal{Z} = \sum_Q \exp\left(-\frac{E_{\mu Q}}{k_B T}\right)$ is the partition function and $\langle v_{\mu Q} \rangle = \partial_Q E_{\mu Q} / \hbar$ is the exciton group velocity. Larger values of $\Gamma_{\mu Q}$ lead to slower excitons due to exciton-phonon scattering. However, as we address in the main text, this effect competes with the group velocity itself, which leads to non-trivial behaviour for topological excitons.

F. Exciton-polaron formation

The full Hamiltonian describing a system hosting excitons and phonons can be written as

$$H = H_{\text{ex},0} + H_{\text{ph},0} + H_{\text{ex-ph}}. \quad (42)$$

To describe the impact of phonons on the excitonic properties, we define a new polaronic Hamiltonian which absorbs the impact of the exciton-phonon coupling into the single-particle energies. Following Ref. [54], we define a polaronic transformation:

$$S = \sum_{Q, K, \nu, \beta} \mathcal{D}_{QK\beta}^{\mu\nu} \left(\frac{1}{E_{\nu Q+K} - E_{\mu Q} + \hbar\Omega_{K\beta}} \hat{\mathbf{b}}_{\beta, -q}^\dagger + \frac{1}{E_{\nu Q+K} - E_{\mu Q} - \hbar\Omega_{K\beta}} \hat{\mathbf{b}}_{\beta, q} \right) \hat{\mathbf{X}}_{Q+K}^{\nu\dagger} \hat{\mathbf{X}}_Q^\mu, \quad (43)$$

which allows us to re-write the Hamiltonian as:

$$\tilde{H} = H_{\text{ex},0} + H_{\text{ph},0} - \frac{1}{2} [S, H_{\text{ex-ph}}]. \quad (44)$$

On solving the commutator, we arrive at the following Hamiltonian:

$$\tilde{H} = H_{\text{ex},0} + H_{\text{ph},0} - \sum_{Q, K, \nu, \beta} |\mathcal{D}_{QK\beta}^{\mu\nu}|^2 \left(\frac{n_K^\beta + 1}{E_{\nu Q+K} - E_{\mu Q} + \hbar\Omega_{K\beta}} + \frac{n_K^\beta}{E_{\nu Q+K} - E_{\mu Q} - \hbar\Omega_{K\beta}} \right) \hat{\mathbf{X}}_Q^{\mu\dagger} \hat{\mathbf{X}}_Q^\mu. \quad (45)$$

The Hamiltonian \tilde{H} can be solved for the phonon-interaction corrected excitonic envelopes $\tilde{\Psi}_{\mu Q}(\mathbf{k})$ on achieving self-consistency with the calculated self-energies $\Sigma_{\mu Q}$, the associated dephasing rates Γ_Q , and the given exciton-phonon interaction matrix elements $\mathcal{D}_{QK\beta}^{\mu\nu}$. Namely, we have $\tilde{E}_{\mu Q} = E_{\mu Q} - \text{Re} \Sigma_{\mu Q}$, with:

$$\text{Re} \Sigma_{\mu Q} = - \lim_{\delta_0 \rightarrow 0} \Re \sum_{K, \nu, \beta} |\mathcal{D}_{QK\beta}^{\mu\nu}|^2 \left(\frac{n_K^\beta + 1}{E_{\nu Q+K} - E_{\mu Q} + \hbar\Omega_{K\beta} + i\Gamma_Q + i\delta_0} + \frac{n_K^\beta}{E_{\nu Q+K} - E_{\mu Q} - \hbar\Omega_{K\beta} + i\Gamma_Q + i\delta_0} \right). \quad (46)$$

We observe a clear polaron shift, as shown in Fig. 5 of the main text, and a minor renormalisation of the excitonic effective mass. Finally, on differentiating the polaron-renormalised band energy $\bar{E}_{\mu Q}$, we obtain:

$$\langle \bar{v}_{\mu Q} \rangle = \frac{1}{\hbar} \partial_Q \bar{E}_{\mu Q}. \quad (47)$$

Here, implicitly, the derivatives of the matrix elements $D_{Q\kappa\beta}^{\mu\nu}$ entering the self-energy $\Sigma_{\mu Q}$ that satisfies a self-consistency condition, allow the excitonic quantum geometry to affect the renormalised exciton transport in the presence of phonons.

Finally, we find that in the presence of exciton-polaron corrections [54, 65], the topology of excitons remains unaltered. Furthermore, the transport in the presence of a non-uniform electric field qualitatively overlaps with the calculation which did not involve the renormalisation with phonons. We show the corresponding results in Fig. 5 of the main text.

-
- [1] Gang Wang, Alexey Chernikov, Mikhail M Glazov, Tony F Heinz, Xavier Marie, Thierry Amand, and Bernhard Urbaszek, “Colloquium: Excitons in atomically thin transition metal dichalcogenides,” *Reviews of Modern Physics* **90**, 021001 (2018).
- [2] Raul Perea-Causin, Daniel Erkensten, Jamie M Fitzgerald, Joshua JP Thompson, Roberto Rosati, Samuel Brem, and Ermin Malic, “Exciton optics, dynamics, and transport in atomically thin semiconductors,” *APL Materials* **10** (2022).
- [3] Katarzyna Posmyk, Mateusz Dyksik, Alessandro Surrente, Duncan K Maude, Natalia Zawadzka, Adam Babiński, Maciej R Molas, Watcharaphol Paritmongkol, Mirosław Maczka, William A Tisdale, *et al.*, “Exciton fine structure in 2d perovskites: The out-of-plane excitonic state,” *Advanced Optical Materials* **12**, 2300877 (2024).
- [4] Oleksandr V Mikhnenko, Paul WM Blom, and Thuc-Quyen Nguyen, “Exciton diffusion in organic semiconductors,” *Energy & Environmental Science* **8**, 1867–1888 (2015).
- [5] Ana M Valencia, Daniel Bischof, Sebastian Anhäuser, Marc Zeplichal, Andreas Terfort, Gregor Witte, and Caterina Cocchi, “Excitons in organic materials: revisiting old concepts with new insights,” *Electronic Structure* **5**, 033003 (2023).
- [6] Alexey Chernikov, Timothy C Berkelbach, Heather M Hill, Albert Rigosi, Yilei Li, Burak Aslan, David R Reichman, Mark S Hybertsen, and Tony F Heinz, “Exciton binding energy and nonhydrogenic Rydberg series in monolayer WS₂,” *Physical review letters* **113**, 076802 (2014).
- [7] Hongyi Yu, Xiaodong Cui, Xiaodong Xu, and Wang Yao, “Valley excitons in two-dimensional semiconductors,” *National Science Review* **2**, 57–70 (2015).
- [8] Mildred S Dresselhaus, Gene Dresselhaus, Riichiro Saito, and Ado Jorio, “Exciton photophysics of carbon nanotubes,” *Annu. Rev. Phys. Chem.* **58**, 719–747 (2007).
- [9] Samuele Giannini, Wei-Tao Peng, Lorenzo Cupellini, Daniele Padula, Antoine Carof, and Jochen Blumberger, “Exciton transport in molecular organic semiconductors boosted by transient quantum delocalization,” *Nature Communications* **13**, 2755 (2022).
- [10] Mark WB Wilson, Akshay Rao, Jenny Clark, R Sai Santosh Kumar, Daniele Brida, Giulio Cerullo, and Richard H Friend, “Ultrafast dynamics of exciton fission in polycrystalline pentacene,” *Journal of the American Chemical Society* **133**, 11830–11833 (2011).
- [11] Daniel N Congreve, Jiye Lee, Nicholas J Thompson, Eric Hontz, Shane R Yost, Philip D Reuswig, Matthias E Bahlke, Sebastian Reineke, Troy Van Voorhis, and Marc A Baldo, “External quantum efficiency above 100% in a singlet-exciton-fission-based organic photovoltaic cell,” *Science* **340**, 334–337 (2013).
- [12] Yuwei Xu, Pei Xu, Dehua Hu, and Yuguang Ma, “Recent progress in hot exciton materials for organic light-emitting diodes,” *Chemical Society Reviews* **50**, 1030–1069 (2021).
- [13] Rituparno Chowdhury, Marco D Preuss, Hwan-Hee Cho, Joshua JP Thompson, Samarpita Sen, Tomi Baikie, Pratyush Ghosh, Yorrick Boeije, Xian-Wei Chua, Kai-Wei Chang, *et al.*, “Circularly polarised electroluminescence from chiral excitons in vacuum-sublimed supramolecular semiconductor thin films,” *arXiv preprint arXiv:2408.13905* (2024).
- [14] Krishnamoorthy Shanmugaraj and S Abraham John, “Water-soluble MoS₂ quantum dots as effective fluorescence probe for the determination of bilirubin in human fluids,” *Spectrochim. Acta A Mol. Biomol. Spectrosc.* **215**, 290–296 (2019).
- [15] Alisha Geldert, Chwee Teck Lim, *et al.*, “Paper-based MoS₂ nanosheet-mediated fret aptasensor for rapid malaria diagnosis,” *Sci. Rep.* **7**, 1–8 (2017).
- [16] Yu Li Huang, Yu Jie Zheng, Zhibo Song, Dongzhi Chi, Andrew TS Wee, and Su Ying Quek, “The organic–2d transition metal dichalcogenide heterointerface,” *Chemical Society Reviews* **47**, 3241–3264 (2018).
- [17] Alexander J Sneyd, Tomoya Fukui, David Paleček, Suryoday Proshan, Isabella Wagner, Yifan Zhang, Jooyoung Sung, Sean M Collins, Thomas JA Slater, Zahra Andaji-Garmaroudi, *et al.*, “Efficient energy transport in an organic semiconductor mediated by transient exciton delocalization,” *Science Advances* **7**, eabh4232 (2021).
- [18] Dominik Muth, Sebastian Anhäuser, Daniel Bischof, Anton Krüger, Gregor Witte, and Marina Gerhard, “Transport, trapping, triplet fusion: thermally retarded exciton migration in tetracene single crystals,” *Nanoscale* **16**, 13471–13482 (2024).
- [19] Mahya Ghorab, Ali Fattah, and Mojtaba Joodaki, “Fundamentals of organic solar cells: A review on mobility issues and measurement methods,” *Optik* **267**, 169730 (2022).
- [20] Darius Gunder, Ana M Valencia, Michele Guerrini, Tobias Breuer, Caterina Cocchi, and Gregor Witte, “Polarization-resolved optical excitation of charge-transfer excitons in pen: Pfp cocrystalline films: limits of nonperiodic modeling,” *The Journal of Physical Chemistry Letters* **12**, 9899–9905 (2021).
- [21] Chen Chen, Liang Wang, Yuandong Sun, Yiwei Fu, Chuanhang Guo, Bojun Zhou, Zirui Gan, Dan Liu, Wei Li, and Tao Wang, “Realizing an unprecedented fill factor of 82.2% in ternary or-

- ganic solar cells via co-crystallization of non-fullerene acceptors,” *Advanced Functional Materials* **33**, 2305765 (2023).
- [22] Stephanie Bettis Homan, Vinod K Sangwan, Itamar Balla, Hadallia Bergeron, Emily A Weiss, and Mark C Hersam, “Ultrafast exciton dissociation and long-lived charge separation in a photovoltaic pentacene–MoS₂ van der Waals heterojunction,” *Nano Letters* **17**, 164–169 (2017).
- [23] Joshua JP Thompson, Victoria Lumsargis, Maja Feierabend, Quichen Zhao, Kang Wang, Letian Dou, Libai Huang, and Ermin Malic, “Interlayer exciton landscape in WS₂/tetracene heterostructures,” *Nanoscale* **15**, 1730–1738 (2023).
- [24] Xiao-Liang Qi and Shou-Cheng Zhang, “Topological insulators and superconductors,” *Rev. Mod. Phys.* **83**, 1057–1110 (2011).
- [25] M. Z. Hasan and C. L. Kane, “Colloquium: Topological Insulators,” *Rev. Mod. Phys.* **82**, 3045–3067 (2010).
- [26] N. P. Armitage, E. J. Mele, and Ashvin Vishwanath, “Weyl and dirac semimetals in three-dimensional solids,” *Rev. Mod. Phys.* **90**, 015001 (2018).
- [27] Fengcheng Wu, Timothy Lovorn, and A. H. MacDonald, “Topological exciton bands in moiré heterojunctions,” *Phys. Rev. Lett.* **118**, 147401 (2017).
- [28] Yves H. Kwan, Yichen Hu, Steven H. Simon, and S. A. Parameswaran, “Exciton band topology in spontaneous quantum anomalous Hall insulators: Applications to twisted bilayer graphene,” *Phys. Rev. Lett.* **126**, 137601 (2021).
- [29] Wojciech J. Jankowski, Joshua J. P. Thompson, Bartomeu Monserrat, and Robert-Jan Slager, “Excitonic topology and quantum geometry in organic semiconductors,” (2024), arXiv:2406.11951 [cond-mat.mes-hall].
- [30] Henry Davenport, Johannes Knolle, and Frank Schindler, “Interaction-induced crystalline topology of excitons,” (2024), arXiv:2405.19394 [cond-mat.mes-hall].
- [31] Jianhua Zhu, Haoxiang Chen, Ji Chen, and Wei Wu, “One-dimensional dexter-type excitonic topological phase transition,” *Phys. Rev. B* **110**, 085418 (2024).
- [32] JP Provost and G Valsecchi, “Riemannian structure on manifolds of quantum states,” *Communications in Mathematical Physics* **76**, 289–301 (1980).
- [33] Adrien Bouhon, Abigail Timmel, and Robert-Jan Slager, “Quantum geometry beyond projective single bands,” (2023), arXiv:2303.02180 [cond-mat.mes-hall].
- [34] Borja Cirera, Ana Sánchez-Grande, Bruno de la Torre, José Santos, Shayan Edalatmanesh, Eider Rodríguez-Sánchez, Koen Lauwaet, Benjamin Mallada, Radek Zbořil, Rodolfo Miranda, *et al.*, “Tailoring topological order and π -conjugation to engineer quasi-metallic polymers,” *Nature nanotechnology* **15**, 437–443 (2020).
- [35] D. Romanin, M. Calandra, and A. W. Chin, “Excitonic switching across a F_2 topological phase transition: From Mott-Wannier to Frenkel excitons in organic materials,” *Phys. Rev. B* **106**, 155122 (2022).
- [36] Junyeong Ahn, Sungjoon Park, Dongwook Kim, Youngkuk Kim, and Bohm-Jung Yang, “Stiefel-Whitney classes and topological phases in band theory,” *Chinese Physics B* **28**, 117101 (2019).
- [37] Adrien Bouhon, Tomáš Bzdusek, and Robert-Jan Slager, “Geometric approach to fragile topology beyond symmetry indicators,” *Phys. Rev. B* **102**, 115135 (2020).
- [38] W. P. Su, J. R. Schrieffer, and A. J. Heeger, “Solitons in polyacetylene,” *Phys. Rev. Lett.* **42**, 1698–1701 (1979).
- [39] W. P. Su, J. R. Schrieffer, and A. J. Heeger, “Soliton excitations in polyacetylene,” *Phys. Rev. B* **22**, 2099–2111 (1980).
- [40] Joshua JP Thompson, Dominik Muth, Sebastian Anhäuser, Daniel Bischof, Marina Gerhard, Gregor Witte, and Ermin Malic, “Singlet-exciton optics and phonon-mediated dynamics in oligocene semiconductor crystals,” *Natural Sciences* **3**, e20220040 (2023).
- [41] Roberto Rosati, Samuel Brem, Raúl Perea-Causín, Robert Schmidt, Iris Niehues, Steffen Michaelis de Vasconcellos, Rudolf Bratschitsch, and Ermin Malic, “Strain-dependent exciton diffusion in transition metal dichalcogenides,” *2D Materials* **8**, 015030 (2020).
- [42] Arjun Ashoka, Nicolas Gauriot, Aswathy V. Girija, Nipun Sawhney, Alexander J. Sneyd, Kenji Watanabe, Takashi Taniguchi, Jooyoung Sung, Christoph Schnedermann, and Akshay Rao, “Direct observation of ultrafast singlet exciton fission in three dimensions,” *Nature Communications* **13** (2022), 10.1038/s41467-022-33647-5.
- [43] Zhilong Zhang, Jooyoung Sung, Daniel TW Toolan, Sanyang Han, Raj Pandya, Michael P Weir, James Xiao, Simon Dowland, Mengxia Liu, Anthony J Ryan, *et al.*, “Ultrafast exciton transport at early times in quantum dot solids,” *Nature Materials* **21**, 533–539 (2022).
- [44] Willy Knorr, Samuel Brem, Giuseppe Meneghini, and Ermin Malic, “Exciton transport in a moiré potential: From hopping to dispersive regime,” *Physical Review Materials* **6**, 124002 (2022).
- [45] Junyeong Ahn, Guang-Yu Guo, Naoto Nagaosa, and Ashvin Vishwanath, “Riemannian geometry of resonant optical responses,” *Nature Physics* **18**, 290–295 (2021).
- [46] Alexey Chernikov and Mikhail M. Glazov, “Chapter three - exciton diffusion in 2d van der waals semiconductors,” in *2D Excitonic Materials and Devices*, Semiconductors and Semimetals, Vol. 112, edited by Parag B. Deotare and Zetian Mi (Elsevier, 2023) pp. 69–110.
- [47] Tamaghna Hazra, Nishchal Verma, and Mohit Randeria, “Bounds on the superconducting transition temperature: Applications to twisted bilayer graphene and cold atoms,” *Phys. Rev. X* **9**, 031049 (2019).
- [48] Yugo Onishi and Liang Fu, “Fundamental bound on topological gap,” *Phys. Rev. X* **14**, 011052 (2024).
- [49] Joshua JP Thompson, Samuel Brem, Marne Verjans, Robert Schmidt, Steffen Michaelis de Vasconcellos, Rudolf Bratschitsch, and Ermin Malic, “Anisotropic exciton diffusion in atomically-thin semiconductors,” *2D Materials* **9**, 025008 (2022).
- [50] Galit Cohen, Jonah B Haber, Jeffrey B Neaton, Diana Y Qiu, and Sivan Refaely-Abramson, “Phonon-driven femtosecond dynamics of excitons in crystalline pentacene from first principles,” *Physical review letters* **132**, 126902 (2024).
- [51] T Markvart and R Greef, “Polaron-exciton model of resonance energy transfer,” *The Journal of chemical physics* **121**, 6401–6405 (2004).
- [52] Kameron R Hansen, C Emma McClure, Daniel Powell, Hao-Chieh Hsieh, Laura Flannery, Kelsey Garden, Edwin J Miller, Daniel J King, Sami Sainio, Dennis Nordlund, *et al.*, “Low exciton binding energies and localized exciton-polaron states in 2d tin halide perovskites,” *Advanced Optical Materials* **10**, 2102698 (2022).
- [53] Michal Baranowski, Andrzej Nowok, Krzysztof Galkowski, Mateusz Dyksik, Alessandro Surrente, Duncan Maude, Marios Zacharias, George Volonakis, Samuel D Stranks, Jacky Even, *et al.*, “Polaronic mass enhancement and polaronic excitons in metal halide perovskites,” *ACS Energy Letters* **9**, 2696–2702 (2024).
- [54] Willy Knorr, Samuel Brem, Giuseppe Meneghini, and Ermin Malic, “Polaron-induced changes in moiré exciton propagation in twisted van der waals heterostructures,” (2024),

- [arXiv:2401.07703 \[cond-mat.mes-hall\]](#).
- [55] Zhenbang Dai, Chao Lian, Jon Lafuente-Bartolome, and Feliciano Giustino, “Excitonic polarons and self-trapped excitons from first-principles exciton-phonon couplings,” *Phys. Rev. Lett.* **132**, 036902 (2024).
- [56] R Coehoorn, L Zhang, PA Bobbert, and H Van Eersel, “Effect of polaron diffusion on exciton-polaron quenching in disordered organic semiconductors,” *Physical Review B* **95**, 134202 (2017).
- [57] Sebastian Hurtado Parra, Daniel B Straus, Bryan T Fichera, Natasha Iotov, Cherie R Kagan, and James M Kikkawa, “Large exciton polaron formation in 2d hybrid perovskites via time-resolved photoluminescence,” *ACS nano* **16**, 21259–21265 (2022).
- [58] Jiabin Yu, Christopher J. Ciccarino, Raffaello Bianco, Ion Errea, Prineha Narang, and B. Andrei Bernevig, “Non-trivial quantum geometry and the strength of electron-phonon coupling,” *Nature Physics* **20**, 1262–1268 (2024).
- [59] Xuzhe Ying and K. T. Law, “Flat band excitons and quantum metric,” (2024), [arXiv:2407.00325 \[cond-mat.mes-hall\]](#).
- [60] Fujiang Yang, Ruixuan Meng, Gaiyan Zhang, Kun Gao, and Shijie Xie, “Migration of an exciton in organic polymers driven by a nonuniform internal electric field,” *Organic Electronics* **30**, 171–175 (2016).
- [61] Swati Chaudhary, Christina Knapp, and Gil Refael, “Anomalous exciton transport in response to a uniform in-plane electric field,” *Physical Review B* **103** (2021), [10.1103/physrevb.103.165119](#).
- [62] Gabriel Antonius and Steven G. Louie, “Theory of exciton-phonon coupling,” *Phys. Rev. B* **105**, 085111 (2022).
- [63] C. Trallero-Giner, E. Menéndez-Proupin, E. Suárez Morell, R. Pérez-Álvarez, and Darío G. Santiago-Pérez, “Phenomenological model for long-wavelength optical modes in transition metal dichalcogenide monolayer,” *Physical Review B* **103** (2021), [10.1103/physrevb.103.235424](#).
- [64] Giuseppe Meneghini, Samuel Brem, and Ermin Malic, “Excitonic thermalization bottleneck in twisted TMD heterostructures,” *Nano Letters* **24**, 4505–4511 (2024).
- [65] Zhenbang Dai, Chao Lian, Jon Lafuente-Bartolome, and Feliciano Giustino, “Excitonic polarons and self-trapped excitons from first-principles exciton-phonon couplings,” *Phys. Rev. Lett.* **132**, 036902 (2024).

SUPPLEMENTAL MATERIAL

Topologically-enhanced exciton transport

Joshua J. P. Thompson,¹ Wojciech J. Jankowski,² Robert-Jan Slager,² and Bartomeu Monserrat^{1,2}

¹*Department of Materials Science and Metallurgy, University of Cambridge, 27 Charles Babbage Road, Cambridge CB3 0FS, United Kingdom*

²*Theory of Condensed Matter Group, Cavendish Laboratory, University of Cambridge, J. J. Thomson Avenue, Cambridge CB3 0HE, United Kingdom*

(Dated: October 3, 2024)

I. FIRST PRINCIPLES CALCULATIONS

We perform density functional theory calculations using the QUANTUM ESPRESSO package [S1, S2] to study the polypentacene chain. We use kinetic energy cutoffs of 80 Ry and 500 Ry for the wavefunction and charge density, respectively, as well as 12 k -points to sample the Brillouin zone along the chain direction. Generalized gradient approximation norm-conserving pseudopotentials in the Perdew-Burke-Ernzerhof formulation were used, which were generated using the code ONCVSP (Optimized Norm-Conserving Vanderbilt PSEUDO Potential) [S3]. These potentials can be found online via the Schlipf-Gygi norm-conserving pseudopotential library [S4]. In order to prevent interactions between periodic images of the organic chain, we include a 34.3 Å spacing in the planar direction perpendicular to the organic polymer chain, as well as a vacuum spacing of 27.52 Å in the out-of-plane direction. Structural optimisation of the atomic coordinates was performed in order to reduce the forces below 0.0015 Ry/Å. The hopping parameters of the Su-Schrieffer-Heeger (SSH) tight-binding model [S5, S6] were deduced from these calculations, following Ref. [S7].

II. DERIVATION OF THE FREE EXCITONIC QUANTUM FOKKER-PLANCK DYNAMICS

In this section we derive the quantum diffusive Fokker-Planck dynamics describing the propagation of free excitons following photoexcitation. The diffusivity associated with exciton propagation enters the Fokker-Planck Gaussian probability distribution capturing the time-dependent propagation as:

$$P(x, x'|t, t') = \frac{1}{\sqrt{2\pi[2D(t-t') + w_0^2]}} \exp\left(-\frac{(x-x')^2}{2[2D(t-t') + w_0^2]}\right), \quad (\text{S1})$$

where w_0 is the width of the initial Gaussian probability distribution and D is the diffusivity, which can be obtained from the quantum mechanical treatment derived from the Heisenberg equation of motion. We note that once the hopping probability amplitudes t_{mj}^v are quantum-mechanically evaluated, which fully captures the relationship between the transport dynamics and the quantum metric, the time-evolution of the exciton density can be formally reduced to a stochastic random-walk problem.

To describe free exciton propagation, we assume that the static lattice of ions fully determines the exciton mass $m \rightarrow m_v^*$, where the mass is band-dependent. The corresponding effective continuum Hamiltonian driving free exciton propagation in one spatial dimension is:

$$\hat{H}_v = -\frac{\hbar^2}{2m_v^*} \partial_x^2. \quad (\text{S2})$$

Inserting the band-projected density $\hat{\rho}^v = \hat{P}_v \hat{\rho} \hat{P}_v$, where $\hat{P}_v = \sum_Q |u_{vQ}^{\text{exc}}\rangle \langle u_{vQ}^{\text{exc}}|$ is a projector onto the exciton band with index v , we obtain the Heisenberg equation:

$$i\hbar \partial_t \hat{\rho}^v = [\hat{H}_v, \hat{\rho}^v]. \quad (\text{S3})$$

Hence, in an effective band-projected picture, we further fit the free excitonic density propagation driven by Heisenberg equation to an exact partial differential equation governing the Fokker-Planck dynamics that yields the Fick's law. Here, on employing the position representation, the fitting reduces to the one-dimensional density diffusion equation:

$$\partial_t \rho^v(x, t) = D_v \partial_x^2 \rho^v(x, t). \quad (\text{S4})$$

On comparing the Heisenberg equation to the diffusion equation, we find:

$$D_v = \frac{\hbar}{2m_v^*}, \quad (\text{S5})$$

where we have performed a Wick rotation to imaginary time $t \rightarrow it$ within the fitting.

With the diffusion equation or the band-projected exciton density $\rho^\nu(x, t)$, as given by Fick's law, we solve the differential equation to obtain a Gaussian solution for propagation:

$$\rho^\nu(x, t) = \frac{1}{\sqrt{2\pi[2D_\nu t + w_0^2]}} \exp\left(-\frac{(x-x')^2}{2[2D_\nu t + w_0^2]}\right). \quad (\text{S6})$$

Recognizing that the expected value of the density can be interpreted as a probability distribution, $\rho^\nu(x, t) \rightarrow P(x, x'|t, t')$, and shifting the initial time $t_{\text{ini}} = 0 \rightarrow t_{\text{ini}} = t'$, we explicitly retrieve a Fokker-Planck propagation for the excitons, with diffusivity being reflected by the quantum mechanics at the level of the effective mass.

Alternatively, we could begin with a lattice-regularized excitonic tight-binding Hamiltonian \hat{H}_{free} , and choose $t_{mj}^\nu = t_{jn}^\nu \equiv t^\nu$. Here, we only consider nearest-neighbor hoppings ($j \pm 1 = m = n$) for simplicity. On inserting into the Heisenberg equation [S8], we obtain:

$$\partial_t \rho^\nu(x, t) \approx \partial_t \rho_{nm}^\nu = -\frac{i}{\hbar} \sum_j (t_{nj}^\nu \rho_{nj} - t_{jn}^\nu \rho_{jn}) \approx -\frac{i}{\hbar} (t^\nu (\rho_{m+1}^\nu - \rho_{n+1}^\nu) + t^\nu (\rho_{m-1}^\nu - \rho_{n-1}^\nu)). \quad (\text{S7})$$

We can also write:

$$\partial_t \rho^\nu(x, t) \approx -\frac{2t^\nu}{\hbar} (\text{Im } \rho_{m+1}^\nu - \text{Im } \rho_{n-1}^\nu), \quad (\text{S8})$$

in terms of the coherences ρ_{nm}^ν ($n \neq m$) of the density matrix. Importantly, we note that the diffusivity D_ν depends on both the hoppings t^ν , which in turn depend only and specifically on the band dispersion $E_\nu(Q)$ (see Methods), and on the coherences, that is, off-diagonal elements of the density matrix. In other words, the hoppings t^ν reflect the intraband excitonic physics driven by the diagonal terms ρ_{nn}^ν , whereas the off-diagonal elements are related to the interband contributions. The latter are given by quantum geometric corrections, which we derive and study further in the next sections.

III. DERIVATION OF THE EXCITON DIFFUSIVITY WITH QUANTUM GEOMETRIC CONTRIBUTIONS

In this section we derive the result for free exciton diffusivity quoted in the Methods of the main text, explicitly:

$$D_\nu = \frac{1}{2\hbar} \left\langle \frac{\partial^2 E_{\nu Q}}{\partial Q^2} \right\rangle + \frac{1}{\hbar} \sum_{\mu \neq \nu} \langle \Delta_{\mu\nu}(Q) g_{xx}^{\mu\nu}(Q) \rangle. \quad (\text{S9})$$

As derived in the previous section, the diffusivity of freely-propagating excitons is given by $D_\nu = \hbar/2m_\nu^*$. Following Ref. [S9], we define the effective mass m_ν^* in exciton band ν and in one dimension as:

$$\frac{1}{m_\nu^*} = \frac{1}{\hbar^2} \langle \partial_Q^2 H_{\text{exc}} \rangle_\nu \equiv \frac{1}{\hbar^2} \frac{\int_{\text{BZ}} dQ \langle u_{\nu Q}^{\text{exc}} | \partial_Q^2 H_{\text{exc}} | u_{\nu Q}^{\text{exc}} \rangle}{\int_{\text{BZ}} dQ}, \quad (\text{S10})$$

where H_{exc} is an effective exciton Hamiltonian associated with the exciton band structure $E_\nu(Q)$ and the exciton Bloch states $|u_{\nu Q}^{\text{exc}}\rangle$. To connect the effective mass to the quantum geometry of excitons, we utilize the Hellmann-Feynman theorem:

$$\begin{aligned} \langle u_{\nu Q}^{\text{exc}} | \partial_Q H_{\text{exc}} | u_{\nu Q}^{\text{exc}} \rangle &= \partial_Q (\langle u_{\nu Q}^{\text{exc}} | H_{\text{exc}} | u_{\nu Q}^{\text{exc}} \rangle) + \langle u_{\nu Q}^{\text{exc}} | H_{\text{exc}} | \partial_Q u_{\nu Q}^{\text{exc}} \rangle + \langle \partial_Q u_{\nu Q}^{\text{exc}} | H_{\text{exc}} | u_{\nu Q}^{\text{exc}} \rangle \\ &= \partial_Q E_\nu(Q) + E_\nu(Q) (\langle \partial_Q u_{\nu Q}^{\text{exc}} | u_{\nu Q}^{\text{exc}} \rangle + \langle u_{\nu Q}^{\text{exc}} | \partial_Q u_{\nu Q}^{\text{exc}} \rangle) = \partial_Q E_\nu(Q), \end{aligned} \quad (\text{S11})$$

where we use product rule and the normalization condition on the Bloch states $\langle u_{\nu Q}^{\text{exc}} | u_{\nu Q}^{\text{exc}} \rangle = 1 \implies 0 = \partial_Q (\langle u_{\nu Q}^{\text{exc}} | u_{\nu Q}^{\text{exc}} \rangle) = \langle \partial_Q u_{\nu Q}^{\text{exc}} | u_{\nu Q}^{\text{exc}} \rangle + \langle u_{\nu Q}^{\text{exc}} | \partial_Q u_{\nu Q}^{\text{exc}} \rangle$. Also using the product rule for the second derivative, which enters the effective mass, we obtain:

$$\begin{aligned} \langle u_{\nu Q}^{\text{exc}} | \partial_Q^2 H_{\text{exc}} | u_{\nu Q}^{\text{exc}} \rangle &= \partial_Q (\langle u_{\nu Q}^{\text{exc}} | \partial_Q H_{\text{exc}} | u_{\nu Q}^{\text{exc}} \rangle) - \langle u_{\nu Q}^{\text{exc}} | \partial_Q H_{\text{exc}} | \partial_Q u_{\nu Q}^{\text{exc}} \rangle - \langle \partial_Q u_{\nu Q}^{\text{exc}} | \partial_Q H_{\text{exc}} | u_{\nu Q}^{\text{exc}} \rangle \\ &= \partial_Q^2 E_\nu(Q) - \sum_\mu \langle \partial_Q u_{\nu Q}^{\text{exc}} | u_{\mu Q}^{\text{exc}} \rangle \langle u_{\mu Q}^{\text{exc}} | \partial_Q H_{\text{exc}} | u_{\nu Q}^{\text{exc}} \rangle - \sum_\mu \langle u_{\nu Q}^{\text{exc}} | \partial_Q H_{\text{exc}} | u_{\mu Q}^{\text{exc}} \rangle \langle u_{\mu Q}^{\text{exc}} | \partial_Q u_{\nu Q}^{\text{exc}} \rangle, \end{aligned} \quad (\text{S12})$$

where we have inserted a resolution of the identity, $1 = \sum_{\mu} |u_{\mu Q}^{\text{exc}}\rangle \langle u_{\mu Q}^{\text{exc}}|$, in the second line. On differentiating the eigenvalue equation $H_{\text{exc}} |u_{\nu Q}^{\text{exc}}\rangle = E_{\nu}(Q) |u_{\nu Q}^{\text{exc}}\rangle$, and taking an inner product with $\langle u_{\mu Q}^{\text{exc}}|$, for $\mu \neq \nu$, we obtain:

$$\langle u_{\mu Q}^{\text{exc}} | \partial_Q H_{\text{exc}} |u_{\nu Q}^{\text{exc}}\rangle = (E_{\nu}(Q) - E_{\mu}(Q)) \langle u_{\mu Q}^{\text{exc}} | \partial_Q u_{\nu Q}^{\text{exc}}\rangle = -\Delta_{\mu\nu}(Q) A_{\mu\nu}^{\text{exc}}(Q), \quad (\text{S13})$$

where $\Delta_{\mu\nu}(Q) = E_{\mu}(Q) - E_{\nu}(Q)$ is the energy difference between the pair of exciton bands μ and ν , and $A_{\mu\nu}^{\text{exc}}(Q) \equiv \langle u_{\mu Q}^{\text{exc}} | \partial_Q u_{\nu Q}^{\text{exc}}\rangle$ is a non-Abelian excitonic Berry connection. Therefore, we can rewrite the previous condition as:

$$\begin{aligned} \langle u_{\nu Q}^{\text{exc}} | \partial_Q^2 H_{\text{exc}} |u_{\nu Q}^{\text{exc}}\rangle &= \partial_Q^2 E_{\nu}(Q) + 2 \sum_{\mu \neq \nu} \Delta_{\mu\nu}(Q) \langle \partial_Q u_{\nu Q}^{\text{exc}} | u_{\mu Q}^{\text{exc}}\rangle \langle u_{\mu Q}^{\text{exc}} | \partial_Q u_{\nu Q}^{\text{exc}}\rangle - E_{\nu}(Q) (\langle \partial_Q u_{\nu Q}^{\text{exc}} | u_{\nu Q}^{\text{exc}}\rangle + \langle u_{\nu Q}^{\text{exc}} | \partial_Q u_{\nu Q}^{\text{exc}}\rangle) \\ &= \partial_Q^2 E_{\nu}(Q) + 2 \sum_{\mu \neq \nu} \Delta_{\mu\nu}(Q) g_{xx}^{\mu\nu}(Q), \end{aligned} \quad (\text{S14})$$

where the last term, which also vanished in the Hellmann-Feynman theorem, arises from the resolution of identity when $\mu = \nu$. In the above expression, we have also used the definition of the exciton quantum metric component $g_{xx}^{\mu\nu}(Q) = g_{xx}^{\nu\mu}(Q) \equiv \langle \partial_Q u_{\nu Q}^{\text{exc}} | u_{\mu Q}^{\text{exc}}\rangle \langle u_{\mu Q}^{\text{exc}} | \partial_Q u_{\nu Q}^{\text{exc}}\rangle$. Averaging over the exciton Brillouin zone (Q -space), we obtain:

$$\frac{1}{m_v^*} = \frac{1}{\hbar^2} \langle \partial_Q^2 E_{\nu}(Q) \rangle + \frac{2}{\hbar^2} \sum_{\mu \neq \nu} \langle \Delta_{\mu\nu}(Q) g_{xx}^{\mu\nu}(Q) \rangle. \quad (\text{S15})$$

Inserting the relation between the effective mass and diffusivity $D_{\nu} = \hbar/2m_v^*$ into this expression, gives the final result:

$$D_{\nu} = \frac{1}{2\hbar} \left\langle \frac{\partial^2 E_{\nu Q}}{\partial Q^2} \right\rangle + \frac{1}{\hbar} \sum_{\mu \neq \nu} \langle \Delta_{\mu\nu}(Q) g_{xx}^{\mu\nu}(Q) \rangle. \quad (\text{S16})$$

IV. COMPARISON OF EXCITON TRANSPORT IN POLYPENTACENE AND POLYANTHRACENE

Previous works have shown that on increasing the number of rings in the polyacene polymer building block, a transition from trivial ($n = 3$) to topological ($n = 5$) electrons/excitons occurs [S7, S10, S11]. In the main text we focus on the $n = 5$ polypentacene system as it is known to host topological electrons and excitons, however for completeness here we compare the exciton transport for polyanthracene ($n = 3$), which host trivial electrons and excitons. We extract t_1 and t_2 in the same way as in the polypentacene case, but for polyanthracene we have that $t_1 > t_2$. We again compare the true case ($t_1 > t_2$) with an artificial topological case ($t_1 < t_2$) to elucidate further the role of topology.

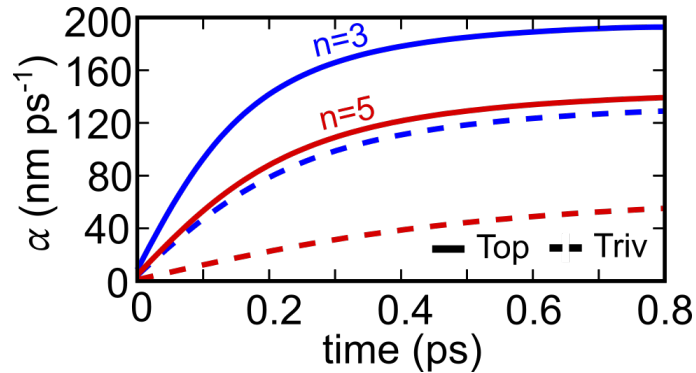


FIG. S1: Comparison of the excitons dispersion velocity on the of topological (*solid*) and trivial excitons (*dashed*) in both polypentacene ($n = 5$), (*red*) and polyanthracene ($n = 3$), (*blue*). We observe that the topological excitons in polyanthracene diffuse freely with higher characteristic velocity.

Comparing the topological and trivial dispersion constants, Fig. S1, we find that exciton propagation in polyanthracene is larger owing to the more dispersive bandstructure and increased screening. Both reduce the dispersion of the excitonic bands and hence lower the diffusion speed. A clear, albeit more modest increase by a factor of 1.6 in the dispersion constant is seen in polyanthracene compared to polypentacene when moving from the trivial to topological regime. Previous works have predicted that the electrons and excitons in polypentacene are topological while those in polyanthracene are trivial, suggesting that the solid red line in Fig. S1 should be compared with the dashed blue line to compare the true ballistic transport in these materials. These indicate that, due to topology, ballistic transport in polypentacene should be marginally faster than in polyanthracene.

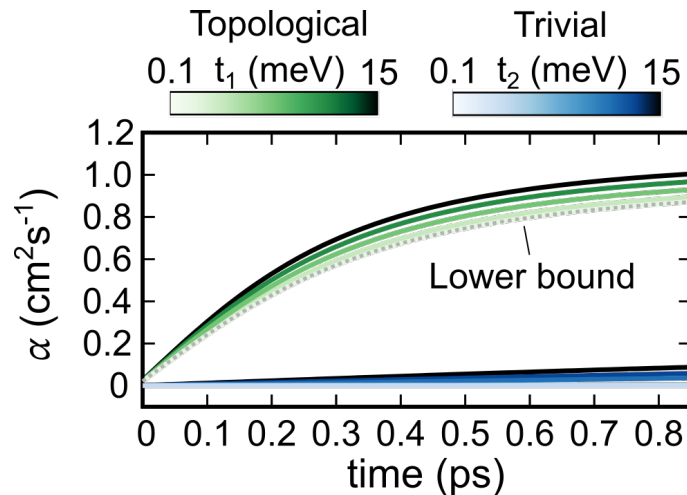


FIG. S2: Exciton dispersion velocity as a function of time for topological (trivial) excitons shown in green (blue) lines for small varying t_1 (t_2) and large fixed t_2 (t_1) equal to 0.5 eV, respectively. The calculated numerical bound on the transport is shown with the grey dotted line.

V. EXCITON TRANSPORT IN THE FLAT BAND REGIME

We perform numerical simulations on polypentacene, while tuning t_1 and t_2 such that one of them is small to reach the flat band regime. Physically, the hoppings can be controlled with an external electrostatic potential, which can be experimentally achieved by chemical functionalisation of the polyacene chain [S10]. This flat band regime for the electronic structure [S5, S6] should host very slow transport [S8]. In the context of the diffusivity derived in the previous part of the Supplemental Material, and in the context of the diffusivity lower bound derived in the Methods, this limit corresponds to vanishing intraband contributions from the band dispersion $\langle \partial_Q^2 E_{vQ} \rangle$, and diffusivity is driven purely by the quantum-geometric contributions.

We show in Fig. S2 that the numerical lower bound (grey dashed line) in the flat-band limits of polypentacene, allows us to manifestly distinguish the quantum-geometric contribution to the diffusivity D_v and velocity parameter α_v , which can be related via the expression, $\alpha_v \approx \hbar/m_v^* \sigma_0 \approx 2D_v/\sigma_0$. Crucially, we observe that trivial excitons, which are not subject to any bounds, exhibit nearly-vanishing α_v and diffusion as expected in the flat-band limit. On the contrary, topological excitons obey the topologically-bounded quantum-geometric diffusivity $D_v = 0.2 \text{ cm}^2/\text{s}$ discussed in the main text. This is true even with a vanishing band dispersion in the flat-band limit. The numerical value was obtained on inserting the topological bound of [S7], lattice parameter $a = 0.6 \text{ nm}$, and minimal gap $\Delta_{\mu\nu} = 0.15 \text{ eV}$, according to the derivation reported in the Methods. With the initial size of the excitonic wavepacket spot $\sigma_0 = 7.5 \text{ nm}$, the peak dispersion velocity of topological excitons is bounded by the value of $\alpha_v \approx \hbar/m_v^* \sigma_0 \approx 2D_v/\sigma_0 \approx 5 \text{ nm/ps}$ in the flat-band limit.

As a final remark, we note that while the band dispersion of trivial excitons allows such excitons to cross the quantum-geometrically bounded peak value of $\alpha_v \approx 5 \text{ nm/ps}$ which topological excitons cannot disobey, we show that the flat-band trivial excitons remain manifestly below this value of peak dispersion velocity, see Fig. S2. This manifestly reflects the trivial excitonic quantum geometry of trivial flat-band excitons, in strong contrast with the topologically-bounded excitonic quantum geometry of topological flat-band excitons.

-
- [S1] P. Giannozzi, S. Baroni, N. Bonini, M. Calandra, R. Car, C. Cavazzoni, D. Ceresoli, G. L. Chiarotti, M. Cococcioni, I. Dabo, A. Dal Corso, S. de Gironcoli, S. Fabris, G. Fratesi, R. Gebauer, U. Gerstmann, C. Gougoussis, A. Kokalj, M. Lazzeri, L. Martin-Samos, N. Marzari, F. Mauri, R. Mazzarello, S. Paolini, A. Pasquarello, L. Paulatto, C. Sbraccia, S. Scandolo, G. Sclauzero, A. P. Seitsonen, A. Smogunov, P. Umari, and R. M. Wentzcovitch, Quantum espresso: a modular and open-source software project for quantum simulations of materials, *Journal of Physics: Condensed Matter* **21**, 395502 (2009).
- [S2] P. Giannozzi, O. Andreussi, T. Brumme, O. Bunau, M. Buongiorno Nardelli, M. Calandra, R. Car, C. Cavazzoni, D. Ceresoli, M. Cococcioni, N. Colonna, I. Carnimeo, A. Dal Corso, S. de Gironcoli, P. Delugas, R. A. DiStasio, A. Ferretti, A. Floris, G. Fratesi, G. Fugallo, R. Gebauer, U. Gerstmann, F. Giustino, T. Gorni, J. Jia, M. Kawamura, H.-Y. Ko, A. Kokalj, E. Küçükbenli, M. Lazzeri, M. Marsili, N. Marzari, F. Mauri, N. L. Nguyen, H.-V. Nguyen, A. Otero-de-la Roza, L. Paulatto, S. Ponce, D. Rocca, R. Sabatini, B. Santra, M. Schlipf, A. P. Seitsonen, A. Smogunov, I. Timrov, T. Thonhauser, P. Umari, N. Vast, X. Wu, and S. Baroni, Advanced capabilities for materials modelling with quantum espresso, *Journal of Physics: Condensed Matter* **29**, 465901 (2017).

- [S3] D. Hamann, Optimized norm-conserving Vanderbilt pseudopotentials, *Physical Review B* **88**, 085117 (2013).
- [S4] M. Schlipf and F. Gygi, Optimization algorithm for the generation of ONCV pseudopotentials, *Computer Physics Communications* **196**, 36 (2015).
- [S5] W. P. Su, J. R. Schrieffer, and A. J. Heeger, Solitons in polyacetylene, *Phys. Rev. Lett.* **42**, 1698 (1979).
- [S6] W. P. Su, J. R. Schrieffer, and A. J. Heeger, Soliton excitations in polyacetylene, *Phys. Rev. B* **22**, 2099 (1980).
- [S7] W. J. Jankowski, J. J. P. Thompson, B. Monserrat, and R.-J. Slager, Excitonic topology and quantum geometry in organic semiconductors (2024), [arXiv:2406.11951 \[cond-mat.mes-hall\]](https://arxiv.org/abs/2406.11951).
- [S8] W. Knorr, S. Brem, G. Meneghini, and E. Malic, Exciton transport in a moiré potential: From hopping to dispersive regime, *Physical Review Materials* **6**, 124002 (2022).
- [S9] Y. Onishi and L. Fu, Fundamental bound on topological gap, *Phys. Rev. X* **14**, 011052 (2024).
- [S10] B. Cirera, A. Sánchez-Grande, B. de la Torre, J. Santos, S. Edalatmanesh, E. Rodríguez-Sánchez, K. Lauwaet, B. Mallada, R. Zbořil, R. Miranda, *et al.*, Tailoring topological order and π -conjugation to engineer quasi-metallic polymers, *Nature nanotechnology* **15**, 437 (2020).
- [S11] D. Romanin, M. Calandra, and A. W. Chin, Excitonic switching across a z_2 topological phase transition: From Mott-Wannier to Frenkel excitons in organic materials, *Phys. Rev. B* **106**, 155122 (2022).